Structural and Multidisciplinary Optimization (2019) 60:2001–2020
https://doi.org/10.1007/s00158-019-02306-7

RESEARCH PAPER

A multi-objective optimization problem in mixed and natural convection for a vertical channel asymmetrically heated

Delphine Ramalingom[1] · **Pierre-Henri Cocquet**[1] · **Rezah Maleck**[1] · **Alain Bastide**[1]

Received: 22 June 2018 / Revised: 30 April 2019 / Accepted: 6 May 2019 / Published online: 3 June 2019

Abstract

This paper deals with a multi-objective topology optimization problem in an asymmetrically heated channel, based on both pressure drop minimization and heat transfer maximization. The problem is modeled by assuming steady-state laminar natural convection flow. The incompressible Navier-Stokes equations coupled with the convection-diffusion equation, under the Boussinesq approximation, are employed and are solved with the finite volume method. In this paper, we discuss some limits of classical pressure drop cost function for buoyancy-driven flow and, we then propose two new expressions of objective functions: the first one takes into account work of pressure forces and contributes to the loss of mechanical power while the second one is related to thermal power and is linked to the maximization of heat exchanges. We use the adjoint method to compute the gradient of the cost functions. The topology optimization problem is first solved for a Richardson (Ri) number and Reynolds number (Re) set respectively to $\mathrm{Ri} \in \{100, 200, 400\}$ and $\mathrm{Re} = 400$. All these configurations are investigated next in order to demonstrate the efficiency of the new expressions of cost functions. We compare two types of interpolation functions for both the design variable field and the effective diffusivity. Both interpolation techniques have pros and cons and give slightly the same results. We notice that we obtain less isolated solid elements with the sigmoid-type interpolation functions. Then, we choose to work with the sigmoid and solve the topology optimization problem in case of pure natural convection, by setting Rayleigh number to $\{3 \times 10^3, 4 \times 10^4, 5 \times 10^5\}$. In all considered cases, our algorithm succeeds to enhance one of the phenomenon modeled by the proposed cost functions without deteriorating the other one. The optimized design obtained suppresses any reversal flow at the exit of the channel. We also show that the thermal exchanges are improved by computing the Nusselt numbers and bulk temperature. We conclude that the new expressions of objective functions are well suited to deal with natural convection optimization problem in a vertical channel.

Keywords Natural convection · Vertical channel · Topology optimization · Objective functions · Adjoint sensitivity analysis · Sigmoid function

1 Introduction

Heat transfer between two vertical plates has applications in many widely used engineering systems; for example, cooling and heating industrial and electronic equipment such as transistors, mainframe computers, plate heat exchangers, and solar energy collectors. Heat transfer by natural convection does not require additional mechanical devices, such as fans, and features robustness and simplicity. So, the concept of natural convection, which is the transport of heat by fluid motion driven by temperature-dependent buoyancy forces, is attractive and the design of efficient heat transfer systems constitute a multiple challenge.

Heat transfer and fluid flows driven by natural convection in open channels have been extensively studied over the last past decades, for vertical or inclined configurations, with uniform heat fluxes or constant temperatures (Elenbaas 1942; Bodoia and Osterle 1962; Aung et al. 1972; Aung 1972; Desrayaud and Lauriat 2009; Sanvicente et al. 2013; Tkachenko et al. 2016; Thebault et al. 2017). Some studies also investigated the optimization of heat transfer in the vertical channel. Bar-Cohen and Rohsenow (1984) perform analytical optimization based on maximizing total heat transfer per unit volume or unit primary area. To achieve this

Responsible Editor: Anton Evgrafov

✉ Delphine Ramalingom
delphine.ramalingom@univ-reunion.fr

[1] Université de La Réunion, Laboratoire PIMENT, 117 Avenue du Général Ailleret, 97430 Le Tampon, France

analytical optimization, they developed composite relations for the variation of the heat transfer coefficient along the plate surfaces. Morrison (1992) developed an approach for determining the optimized fin configurations for a given heat sink in natural convection. The proposed algorithm allows the computer to look for the lowest temperature performance of a user specified range of fin geometries. Nasri et al. (2015) performed a numerical study in order to analyze the effect of adding a chimney to a vertical open channel. They determined the optimal geometric parameters of the chimney and studied thermal and dynamic aspects of the channel-chimney system by varying the width and the height of the chimney while the aspect ratio of the channel is kept fixed. Lim et al. (2018) applied a CFD-based shape optimization in order to find the optimal channel cross-sectional shape for minimizing local heat flux on the cooling surface in fusion divertors. Maximum heat flux on the cooling channel surface is defined as the objective function in the optimization process. Finally, it is found that the maximum heat flux and temperature in the cooling channel can be significantly reduced compared with the original circular channel shape by simple modification of the ellipse-shaped cross section. Talukdar et al. (2019) focused on the optimization of the thermal performance for compressible laminar natural convection flow induced under high-temperature difference in an open-ended vertical channel by optimizing the channel inter-plate spacing using numerical simulation. From the results obtained, a correlation for optimum aspect ratio with Rayleigh number which maximizes the heat transfer within the channel is presented. To summarize, among these different studies, there are few optimization of natural convection heat transfer in open-ended channels investigations other than parametric geometry with few design variables. However, the optimization of these systems simultaneously demands compactness, efficiency and control of heat and mass transfers. As a result, in this paper, we deal with some topology optimization problems for heat and mass transfers, considering the physical case of an asymmetrically heated vertical channel.

Topology optimization is a powerful and a popular tool for designers and engineers to design process. Its notion was initially introduced in structural mechanics by Bendsøe and Kikuchi (1988). In order to increase the structural stiffness under certain load, they targeted the optimal material density distribution by identifying areas in which material should be added. They expressed the design problem in terms of real valued continuous function per point, with values ranging from zero (indicating the presence of void/absence of material) to unity (indicating solid). The method has then been developed to numerous problems in structural mechanics (Sigmund and Maute 2013; Eschenauer and Olhoff 2001; Liang 2007; Hassani and Hinton 1998a, b, c; Wang et al. 2003). In fluid mechanics, the same idea was adapted to Stokes flows by Borrvall and Petersson (2003), by introducing a parameter γ that depends on both the dynamic viscosity ν of the fluid and the specific permeability κ of the porous material: $\gamma = \nu/\kappa$. This parameter γ is often referred to as an inverse permeability function in the literature (Guest et al. 2004). The friction force acting on the fluid by the material is proportional to the velocity of the fluid as $f = -\gamma\vec{u}$ where $\vec{u}$ is the velocity of the fluid. This term is added to the flow equations. Domain areas corresponding to the fluid flow are those where γ is closed to 0 while areas where γ is far from 0 define the part of the domain to be solidified. The optimal solid walls to be designed correspond to the interfaces between the two aforementioned areas. To summarize, the goal of topology optimization is to compute the optimal γ field in order to minimize some objective function under consideration. Contrary to topology optimization applied to design structure, research on topology optimization applied to heat transfer and fluid dynamics is quite recent. Dbouk (2017) presented a review about topology optimization design methods that have been developed for heat transfer systems, and for each of them, he presented their advantages, limitations, and perspectives. In topology optimization problems with large number of design variables, gradient-based algorithms are frequently used to compute accurate solutions efficiently (Othmer 2014; Marck et al. 2013; Alexandersen et al. 2014; Koga et al. 2013; Bruns 2007; Yoon 2010). This algorithm starts with a given geometry and iterates with information related to the derivatives (sensitivity derivatives) of the objective function with respect to the design variables. Among the methods used to compute the sensitivity derivatives required by gradient-based methods, the adjoint method (Othmer 2014, 2008; Kontoleontos et al. 2013; Papoutsis-Kiachagias and Giannakoglou 2016; Marck et al. 2013; Bastide et al. 2018) has received a lot of attention since the cost of computing the necessary derivatives is independent from the number of design variables. Papoutsis-Kiachagias and Giannakoglou (2016) present a review on continuous adjoint method applied to topology optimization for turbulent flows. Tong et al. (2018) have recently discussed on the optimization of thermal conductivity distribution for heat conduction enhancement. They considered different cost functions and demonstrated that they should be carefully chosen when heat conduction is involved. Othmer (2008) derived the continuous adjoint formulations and the boundary conditions on ducted flows for typical cost functions. He proposed an objective function to reduce pressure drops in open cavity. The originality of his method is the versatility of the formulation where the adjoint boundary conditions were expressed in a form that can be adapted to any commonly used objective function. Then, for

the automotive industry, Othmer et al. (2006) implemented several objective functions like dissipated power, equal mass flow through different outlets and flow uniformity. To describe the transition and interface between fluid and solid regions in the domain, the Solid Isotropic Material with Penalization (SIMP) technique (Bendsøe and Kikuchi 1988; Zhou and Rozvany 1991) is the mostly used in the literature as the interpolation technique in topology optimization. This approach represents the non-fluid regions as infinitely stiff, a penalty to the flow, such that no interaction is modeled. A new method of interpolation was presented by Ramalingom et al. (2018) in order to improve the fluid-solid interface during the optimization process. They proposed two sigmoid functions to interpolate material distribution and effective diffusivity. They showed that the transition zones, i.e., zones where the velocity of fluid is not small enough to be considered as solid, can be made arbitrary small. The present paper thus also aims to present an efficient gradient-based optimization method and gives comparison between two types of interpolation functions, namely SIMP and the sigmoids from Ramalingom et al. (2018), for the material distribution and the effective diffusivity.

Conjugate heat transfer was originally treated in Dede (2009) and Yoon (2010). It is worth noting that this field of research is very active today (Haertel et al. 2015; Yaji et al. 2016; Rokicki et al. 2016; Qian and Dede 2016; Haertel and Nellis 2017; Goeke and Wünsch 2017). Most of these works focused on forced convection although authors have previously presented a density-based approach for natural convection problems (Alexandersen et al. 2014; Alexandersen et al. 2015; Saglietti et al. 2017; Pietropaoli et al. 2019). Coffin and Maute (2016) introduced a topology optimization method for 2D and 3D, steady-state, and transient heat transfer problems that are dominated by natural convection in the fluid phase. The geometry of the fluid-solid interface is described by an explicit level-set method. Recently, Alexandersen et al. (2016) used topology optimization to the design of three-dimensional heat sinks cooled by natural convection. Heat sinks in a closed cooled cavity are investigated for several Grashof numbers. Interesting design features are observed and trends are discussed. Joo et al. (2017) presented a density-based method for a simplified convection model for plane extruded structures. Alexandersen et al. (2018) show that the optimized designs obtained thanks to topology optimization for passive cooling of light-emitting diode (LED) lamps by natural convection yield less package temperature with less material compared with a lattice-fin design. Saglietti et al. (2017) considered numerically the natural convection-driven flow in a differentially heated cavity using three different Prandtl numbers ranging from 0.7 to 7 at super-critical conditions. For specific cases, the computation of optimal initial conditions leads to a degenerate problem and the power iteration converges very slowly and fails to extract all possible optimal initial conditions. Lei et al. (2018) used a natural convection experimental setup to study the performance of the fabricated heat sinks, designed by a previously reported topology optimization model for natural convection. The results show that the tested topology optimization heat sinks can always realize the best heat dissipation performance compared with pin-fin heat sinks, when operating under the conditions used for the optimization. Saglietti et al. (2018) studied innovative designs of heat sinks generated through numerical optimization. They investigated the impact of boundary conditions, initial designs, and Rayleigh number. They showed that as the Rayleigh number increases, the topology of the heat exchanger is able to substantially enhance the convection contribution to the heat transfer.

Although well-performing structures are obtained using density-based approach, Alexandersen et al. (2016, 2018) specified that the performance of structures obtained for natural convection cannot be guaranteed in general due to the simplified modeling. In Alexandersen et al. (2014), they treated several difficulties that would be encountered when dealing with natural convection problems as the oscillatory behavior of the solver, namely a damped Newton method, used for the optimization computations. He also reported intermediate relative densities that amplified the natural convection effects leading to non-vanishing velocity in some solid parts of the computational domain. Although it is reported that this issue only arose when the objective function was directly dependent on the velocity field, those zones are considered as solid by the optimization algorithm while they should be treated as fluid. In addition to this, topology optimization of natural convection problems is computationally expensive (Asmussen et al. 2018). Bruns (2007) applied topology optimization to convection-dominated heat transfer problems. He highlighted numerical instabilities in convection-dominated diffusion problems and justified them by the density-design-variable-based topology optimization. Other numerical issues are encountered in topology optimization problems, as checkerboards pattern and intermediate density regions. Authors usually adopted a continuation strategy where the parameter involved in the SIMP interpolation of the effective diffusivity is gradually increased during the optimization process. These values are chosen to aggressively penalize intermediate densities with respect to effective diffusivity and to confine the maximum impermeability to the fully solid parts of the domain. Similarly, authors used filtering techniques (Lazarov and Sigmund 2011; Bruns 2005; Lee 2012; Marck et al. 2013; Alexandersen et al. 2014) to overcome bad connectivity between elements of solid domain. The filtering is done by looking at the "neighborhood" of the individual

element which is defined as the set of elements with centers within the filter radius. Bruns (2005) explained that the main disadvantage of filtering the sensitivities is that the approach is heuristic (Sigmund and Maute 2012) because the sensitivities are not consistent with the primal analysis. Therefore, the optimization problem is not well posed in a rigorous sense. Alexandersen et al. (2013) explained that some form of filtering can be beneficial for some topology optimization problems. Minimizing the energy dissipated in fluid flow problems are generally well posed and no filtering is needed. On the contrary, alternating solid and fluid elements can exist in structural and heat transfer problems but the latter creates areas of solid elements not correctly connected. Sigmund (2007) described various filters type to fix this problem. More recently, Saglietti et al. (2018) investigated a complete conjugated problem in which the effect of the solid material on the surrounding flow through the action of a Brinkman friction term in the Navier-Stokes equations is described. They applied advanced filtering techniques for enforcing a desired length scale to the solid structure. In this paper, we are going to avoid the use of filtering methods and we do not obtain isolated pieces of material at the end of the optimization process. Finally, conjugate and heat transfer optimization problems are dealt with quite many and various single or multi-objective functions, such as thermal compliance (Yoon 2010; Alexandersen et al. 2014, 2015; Joo et al. 2017), mean temperature (Dede 2009), total fluid power dissipated (Dede 2009; Qian and Dede 2016), mass flow through a surface (Alexandersen et al. 2014), heat flux through a surface (Saglietti et al. 2018; Pietropaoli et al. 2019), kinetic energy and the entransy (Saglietti et al. 2018), average temperature at the heat flux region (Coffin and Maute 2016; Haertel et al. 2015; Zhao et al. 2018), mechanical energy (Pietropaoli et al. 2019), dissipation energy combined with pressure drop (Yaji et al. 2016; Qian and Dede 2016), and conductance (Haertel and Nellis 2017).

This paper deals with the minimization of pressure drop and the maximization of heat transfer in a natural convection optimization problem. After analyzing some limits we identified for the classical pressure drop cost function when dealing with flows dominated by natural convection forces, we investigate new expressions of objective functions defined according to a systemic approach to an asymmetrically heated vertical channel. The geometry considered here is the model proposed by Desrayaud et al. (2013) and corresponds to a boundary layer flow with a reversal flow at the exit (Ramalingom et al. 2017). Several configuration cases are considered in order to evaluate the new objective functions. We also compare two types of interpolation functions (sigmoid- and Ramp-type) to interpolate material distribution and effective diffusivity. We then solve the optimization problem in mixed convection, for various Richardson numbers $\mathrm{Ri} = \{100, 200, 400\}$ and then, we deal with the optimization problem in case of pure natural convection, for various Rayleigh numbers $\mathrm{Ra}_b = \{3\times10^5, 4\times10^5, 5\times10^5\}$. Our optimization algorithm succeeds especially to avoid the existence of a reversal flow. We show that our optimized designs increase thermal exchanges by computing the Nusselt numbers. We finally end this paper by drawing some conclusions.

2 Governing equations

The flows considered in this paper are assumed to be in a steady-state laminar regime, newtonian and incompressible. Figure 1 shows the configuration of the computational domain Ω. Physical properties of the fluid are the kinematic viscosity ν and the thermal conductivity λ_f. First, parameters governing the flow for natural convection dominant is the Reynolds number defined as

$$\mathrm{Re} = \frac{Ub}{\nu},$$

with b being the width of the channel and U the reference velocity based on the average velocity at the channel

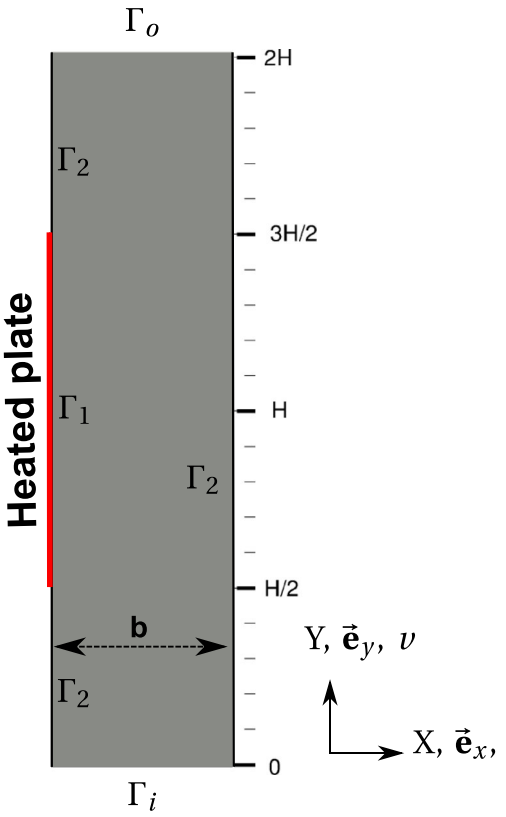

Fig. 1 Geometry of the problem

entrance. In case of pure natural convection, the reference velocity is defined as

$$U_{CN} = \frac{k\ Ra^{1/2}}{b},$$

with k the thermal diffusivities of the fluid. The Prandtl number is the ratio between the momentum and thermal diffusivities of the fluid and is defined as

$$\mathrm{Pr} = \frac{\nu}{k}.$$

In this paper, we consider only fluids with small Prandtl hence satisfying $\mathrm{Pr} < 1$. The Grashof number represents the ratio between buoyancy and viscous force and is defined as

$$\mathrm{Gr}_b = \frac{g\beta\Delta T b^3}{\nu^2},$$

where $\Delta T = -\phi/\lambda_f$ and ϕ is the thermal flux on Γ_1. The modified Rayleigh number is associated with buoyancy-driven flow, also known as natural convection. It is defined as

$$\mathrm{Ra}_b = \mathrm{Gr}_b\mathrm{Pr}.$$

In thermal convection problems, the Richardson number represents the importance of natural convection relative to the forced convection. The latter is given by

$$\mathrm{Ri} = \frac{\mathrm{Gr}_b}{\mathrm{Re}^2}.$$

Note that values greater than unity means that the flow is dominated by natural convection. Under these assumptions and thanks to a method given in Borrvall and Petersson (2003), the porosity field is introduced in the steady-state Navier-Stokes equation as a source term $h_\tau(\gamma)\mathbf{u}$ which yields a Brinkman-like model with a convection term (Ramalingom et al. 2018). Therefore, the dimensionless form of the Navier-Stokes and energy equations are written as follows:

$$\begin{aligned} \nabla\cdot\mathbf{u} &= 0 && \text{in } \Omega,\\ (\mathbf{u}\cdot\nabla)\mathbf{u} &= -\nabla p + \mathrm{A}\Delta\mathbf{u} - h_\tau(\gamma)\mathbf{u} + \mathrm{B}\theta\overrightarrow{e_y} && \text{in } \Omega,\\ \nabla\cdot(\mathbf{u}\theta) &= \nabla\cdot(\mathrm{C}k_\tau(\gamma)\nabla\theta) && \text{in } \Omega, \end{aligned} \tag{1}$$

where the constants A, B, C are defined according to the case considered and read

- for dominant natural convection $\{\mathrm{A},\mathrm{B},\mathrm{C}\} = \{\mathrm{Re}^{-1},\ \mathrm{Ri},\ \mathrm{Re}^{-1}\mathrm{Pr}^{-1}\}$,
- for pure natural convection $\{\mathrm{A},\mathrm{B},\mathrm{C}\} = \{\mathrm{Pr}\,\mathrm{Ra_b}^{-1/2},\ \mathrm{Pr},\ \mathrm{Ra_b}^{-1/2}\}$.

In (1), $(\mathbf{u}, p, \theta)$ correspond respectively to the dimensionless velocity, pressure and temperature and are usually referred to as the primal variable in the current setting. Parameter γ is the effective inverse permeability that is going to be determined thanks to the optimization algorithm. For the natural-dominated convection problem, one has the following boundary conditions:

$$\begin{aligned} &\mathbf{u} = 0, && \nabla p = 0, && \partial_n\theta = -1 && \text{on } \Gamma_1,\\ &\mathbf{u} = 0, && \nabla p = 0, && \partial_n\theta = 0 && \text{on } \Gamma_2,\\ &\mathbf{u} = u_i\mathbf{e}_y, && \nabla p = 0, && \theta = 0 && \text{on } \Gamma_i,\\ &\partial_n\mathbf{u} = 0, && p = 0, && \partial_n\theta = 0 && \text{on } \Gamma_o, \end{aligned} \tag{2}$$

where ∂_n is the normal derivative defined as $\partial_n = n\cdot\nabla$, Γ_1, Γ_2, Γ_i, and Γ_o are respectively the hot plate, the adiabatic plates, the inlet and the outlet of the channel. For the natural convection case, the boundary conditions reads as follow:

$$\begin{aligned} &\mathbf{u} = 0, && \nabla p = 0, && \partial_n\theta = -1 && \text{on } \Gamma_1,\\ &\mathbf{u} = 0, && \nabla p = 0, && \partial_n\theta = 0 && \text{on } \Gamma_2,\\ &\partial_n\mathbf{u} = 0, && \nabla p = 0, && \theta = 0 && \text{on } \Gamma_i,\\ &\partial_n\mathbf{u} = 0, && p = 0, && \partial_n\theta = 0 && \text{on } \Gamma_o, (\text{if } \mathbf{u}\cdot\mathbf{n} > 0)\\ &\partial_n\mathbf{u} = 0, && p = -1/2\,\mathbf{u}^2, && \partial_n\theta = 0 && \text{on } \Gamma_o, (\text{if } \mathbf{u}\cdot\mathbf{n} < 0). \end{aligned} \tag{3}$$

According to the results presented by recent studies (Desrayaud et al. 2013; Brangeon et al. 2015; Ramalingom et al. 2017), pressure boundary conditions at the top and bottom sections based on Local Bernoulli relation are chosen in the current numerical study.

3 Topology optimization formulation

The main goal of this paper is to deal with a multi-objective optimization problem in the asymmetrically heated channel. In the literature, cost functions are often expressions of the work of forces or powers that one either wish to minimize or wish to maximize. In the present study, we consider both pressure drop minimization described by a first objective function $\mathcal{J}_1$ and heat transfer maximization described by a second objective function $\mathcal{J}_2$. The optimization problem can then be stated as:

$$\begin{aligned} &\min\ \mathcal{J}(\mathbf{u}, p, \theta) = \mathrm{c}_1\,\mathcal{J}_1(\mathbf{u}, p, \theta) + \mathrm{c}_2\,\mathcal{J}_2(\mathbf{u}, p, \theta),\\ &\qquad \text{where } (\mathbf{u}, p, \theta) \text{ satisfy (1), (2),} \end{aligned} \tag{4}$$

and the cost function $\mathcal{J}$ is the combination of the two objectives functions, c_1 and c_2 are weighting coefficients. It is easy to observe that, for $\mathrm{c}_1 \gg \mathrm{c}_2$, the multi-objective function amounts to a minimum power dissipation problem, while for $\mathrm{c}_1 \ll \mathrm{c}_2$, a maximum heat dissipation problem is defined.

3.1 Multi-objective optimization

In multi-objective optimization, one of the challenges is to benefit from both objective functions. As introduced in previous subsection, the objective function based on maximization of thermal exchanges can involve the increase of pressure drop and conversely for the objective function relative to the dissipation of power. Before combining linearly the two functions, they must then be rescaled to have the same order of magnitude. This can be done by using an Aggregate Objective Function (AOF), also known as the weighted-sum approach, which is based on a linear combination of both objective functions (Athan and Papalambros 1996; Messac et al. 2000). The latter reads:

$$\hat{f} = \frac{f - f_{\min}}{f_{\max} - f_{\min}} \tag{5}$$

where f is either $\mathcal{J}_1$ or $\mathcal{J}_2$. As explained by (Marck et al. 2013), the other four parameters are determined by solving both optimization problems independently (4) for min $\mathcal{J}_1$ and max $\mathcal{J}_2$. Consequently, both rescaled objective functions are ranged between 0 and 1. Such a rescaling allows to consider the following linear combination:

$$\hat{\mathcal{J}} = \omega\, \hat{\mathcal{J}}_1 - (1-\omega)\hat{\mathcal{J}}_2 \tag{6}$$

where $\omega \in [0, 1]$ is the weight balancing the influence of each objective function. Note that this combination involves the opposite of $\mathcal{J}_2$ since one aims at minimizing the combinatory function $\hat{\mathcal{J}}$. Thereafter, $\hat{\mathcal{J}}_1$ and $\hat{\mathcal{J}}_2$ are used only during the optimization process.

3.2 Limits of classical pressure drop cost function for buoyancy-driven flow

In this section, we discuss some limits we identified of the classical pressure drop cost function when dealing with flows dominated by natural convection forces. The latter is widely used in the literature (Borrvall and Petersson 2003; Marck et al. 2013; Othmer 2008; Lv and Liu 2018; Koga et al. 2013; Qian and Dede 2016; Ramalingom et al. 2018) and reads

$$f_1(\mathbf{u}, p) = \int_\Gamma -\mathbf{n}\cdot\mathbf{u}\left(p + \frac{1}{2}|\mathbf{u}|^2\right) \mathrm{d}S. \tag{7}$$

Also, as pointed out by Lv and Liu (2018), it is equivalent to minimize the power dissipated by the fluid when the fluid passes the boundary with constant velocity. It is worth noting that all the previously mentioned studies using cost function (7) does not consider buoyancy-driven flows. We are now going to show that f_1 is no longer the power dissipated by the fluid in the current setting. Starting with a Green formula, we obtain

$$\begin{aligned}
f_1(\mathbf{u}, p) &= -\int_\Gamma \left(p + \frac{1}{2}|\vec{u}|^2\right)\vec{u}\cdot\vec{n}\,\mathrm{d}S \\
&= -\int_\Omega \mathrm{div}\left(\left(p + \frac{1}{2}|\vec{u}|^2\right)\vec{u}\right)\mathrm{d}\Omega \\
&= -\int_\Omega \mathrm{div}\,(\vec{u})\left(p + \frac{1}{2}|\vec{u}|^2\right)\mathrm{d}\Omega \\
&\quad -\int_\Omega \vec{u}\cdot\nabla\left(p + \frac{1}{2}|\vec{u}|^2\right)\mathrm{d}\Omega \\
&= -\int_\Omega \vec{u}\cdot(\nabla p + (\vec{u}\cdot\nabla)\vec{u})\,\mathrm{d}\Omega,
\end{aligned}$$

where we used that $\vec{u}\cdot\{(\vec{u}\cdot\nabla)\vec{u}\} = \vec{u}\cdot(\frac{1}{2}\nabla|\vec{u}|^2)$. Using then (1) and the boundary conditions (2), we infer

$$\begin{aligned}
f_1(\mathbf{u}, p) &= -\int_\Omega \vec{u}\cdot\left(\mathrm{Re}^{-1}\Delta\vec{u} + Ri\theta\vec{e}_y - h_\tau(\gamma)\vec{u}\right)\mathrm{d}\Omega \\
&= \int_\Omega \mathrm{Re}^{-1}|\nabla\vec{u}|^2 + h_\tau(\gamma)|\vec{u}|^2\,\mathrm{d}\Omega \\
&\quad -\int_\Gamma \mathrm{Re}^{-1}\partial_{\vec{n}}\vec{u}\cdot\vec{u}\,d\Gamma - \mathrm{Ri}\int_\Omega(\vec{u}\cdot\vec{e}_y)\theta\,\mathrm{d}\Omega \\
&= \int_\Omega \mathrm{Re}^{-1}|\nabla\vec{u}|^2 + h_\tau(\gamma)|\vec{u}|^2 - \mathrm{Ri}(\vec{u}\cdot\vec{e}_y)\theta\,\mathrm{d}\Omega \\
&\quad -\mathrm{Re}^{-1}\int_{\Gamma_i}(\partial_{\vec{n}}\vec{u}\cdot\mathbf{e}_y)u_i\,\mathrm{d}S.
\end{aligned}$$

From the previous computations, one can see that f_1 indeed represent either the pressure loss inside the channel or the dissipated power but only if the velocity of the fluid is constant across the inlet (hence $\partial_{\vec{n}}\vec{u}\cdot\mathbf{e}_y = 0$) and if $\mathrm{Ri} = 0$. It is worth mentioning that the cost function f_1 can still be used to reduce the total pressure losses in the channel for fairly small Richardson number (see, e.g., Ramalingom et al. 2018 where one has $\mathrm{Ri} = 2.8$). Nevertheless, since in this paper we are going to work with large Ri, that is, $\mathrm{Ri} \geq 100$, we introduce in the next section a new expression for the dissipated power.

3.3 Definition of the cost functions with systemic approach

In our study, we propose to evaluate mechanical and thermal power via two new expressions of both cost functions. We emphasize that proposing another expression of the mechanical power is motivated by the results of Section 3.2 which show analytically that the usual expression of the power dissipated by the fluid (see (7)) actually depends on the Richardson number and does not suit when this number is relatively large. The definition of our new cost function is based on a systemic approach and have the major advantage that they can be used with mean values at input and at output of a given physical model. As a result, as our numerical

results show, they do not seem to suffer from intrinsic limitations coming from the modeling considered.

As we will show below, these functions actually give an optimized design without using any filtering techniques. Moreover, we do not observe isolated pieces of material at the end of the optimization process.

As illustrated in Fig. 2, for a system with an inlet, an outlet, an average velocity (U_i, U_o) and an average temperature (θ_i, θ_o), the thermal power is defined as the product of the mass flow, the volume heat capacity, and the difference of temperature between the entrance and the exit of the system. Likewise, mechanical power is defined as the product of mass flow rate and the difference of total pressure (p_t) between the entrance and the exit of the system. In that way, we chose to minimize the work of pressure forces to minimize the power dissipated in the channel as it is usually done in systemic approach. Hence, the first cost function can be written as:

$$\begin{aligned}\mathcal{J}_1(\mathbf{u}, p) = &-\frac{1}{|\Gamma_i|}\int_{\Gamma_i} p_t \,\mathrm{d}S \int_{\Gamma_i} \mathbf{u}\cdot\mathbf{n}\,\mathrm{d}S \\ &-\frac{1}{|\Gamma_o|}\int_{\Gamma_o} p_t \,\mathrm{d}S \int_{\Gamma_o} \mathbf{u}\cdot\mathbf{n}\,\mathrm{d}S,\end{aligned} \tag{8}$$

where $p_t = p + 1/2\,|\mathbf{u}|^2$ is the total pressure, Γ_i and Γ_o are respectively the entrance (inlet) and the exit (outlet) of the channel and $|S|$ denotes the length of $S \subset \Gamma$.

The second cost function concerns thermal exchange maximization and is given by:

$$\begin{aligned}\mathcal{J}_2(\mathbf{u}, \theta) = &\frac{1}{|\Gamma_i|}\int_{\Gamma_i} \theta \,\mathrm{d}S \int_{\Gamma_i} \mathbf{u}\cdot\mathbf{n}\,\mathrm{d}S \\ &+\frac{1}{|\Gamma_o|}\int_{\Gamma_o} \theta \,\mathrm{d}S \int_{\Gamma_o} \mathbf{u}\cdot\mathbf{n}\,\mathrm{d}S.\end{aligned} \tag{9}$$

We can observe that this systemic approach for defining the cost functions enables to dissociate total pressure or temperature from the mass flow rate, since velocity profile is imposed at the entrance.

Remark 1 Another classical cost function used for instance in Marck et al. (2013) and Kontoleontos et al. (2013) is related to the thermal power thanks to the next expression:

$$f_2(\mathbf{u}, \theta) = \int_{\Gamma} \mathbf{n}\cdot\mathbf{u}\,\theta \,\mathrm{d}S. \tag{10}$$

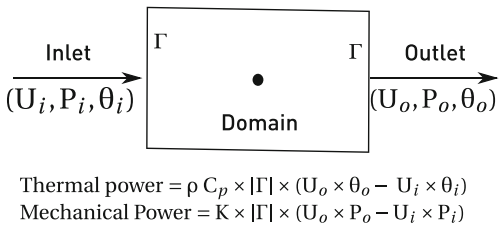

Fig. 2 Systemic approach

Note that maximize f_2 is equivalent to maximize the bulk temperature. Also, maximizing (9) is equivalent to maximize the mean temperature at apertures as opposed to (10).

4 Topology optimization methods

Applying topology optimization to this problem aims to minimize an objective function $\mathcal{J}$ by finding an optimal distribution of solid and fluid element in the computational domain. The goal of topology optimization is to end up with binary designs, i.e., avoid that the design variables take other value than those representing the fluid or the solid. This is usually carried out by penalizing the intermediate densities with respect to the material parameters, such as inverse permeability and effective diffusivity. A standard approach is to use interpolation functions. We are also going to use gradient-based algorithm that relies on the continuous adjoint method.

4.1 Interpolation functions

The additional term $h_\tau(\gamma)$ in (1) physically corresponds to the ratio of a kinematic viscosity and a permeability. As proposed by Guest et al. (2004), Sigmund (2007), and Zhao et al. (2018), a projection approach is employed to relate the element-based design variables to the physical densities firstly and to the thermal diffusivity, secondly. We defined two smooth regularization of Heaviside functions for these interpolations. The interpolation function for the thermal diffusivity of each element is $k_\tau(\gamma)$, both functions were defined in Ramalingom et al. (2018) where it is shown that the intermediate zones can be as small as desired. Regions with very high permeability can be considered as solid regions, and those with low permeability regions are interpreted as pure fluid.

Inverse permeability can be interpolated with the following formula

$$h_\tau(\gamma) = \gamma_{\max}\left(\frac{1}{1+\mathrm{e}^{-\tau(\gamma-\gamma_0)}} - \frac{1}{1+\mathrm{e}^{\tau\gamma_0}}\right) \tag{11}$$

where γ_0 is the abscissa slope of the sigmoid function, τ is the slope of the sigmoid function, and $\gamma_{\max}$ is the maximum value that the design parameter γ can take. In (Ramalingom et al. 2018), it is shown that the parameter γ_0 is linked to the quantity of material added in the domain Ω. These parameters are going to be given in the next section. The difference in the adimensional thermal diffusivities of the fluid and solid regions considered

through the interpolation of effective diffusivity k_τ as follows:

$$k_\tau(\gamma) = \frac{1}{k_f}\left[k_f + (k_s - k_f)\frac{h_\tau(\gamma)}{\gamma_{\max}}\right], \tag{12}$$

where k_s and k_f are respectively the thermal diffusivity of solid and fluid domains.

In this paper, we also studied the impact of a Ramp-type interpolation function on solutions of the optimization problem. The latter has been introduced in Borrvall and Petersson (2003) and can be defined as follows:

$$\sigma(\gamma) = \sigma_{\max} + (\sigma_{\min} - \sigma_{\max})\,(1-\gamma)\,\frac{1+q}{1-\gamma+q}, \tag{13}$$

where $\sigma \in \{h, k\}$ is either the inverse permeability or the thermal diffusivity, $q \to 0$, $\gamma \in [0; \gamma_{\max}]$, $h_{\min} = \gamma_{\min}$, $h_{\max} = \gamma_{\max}$, $k_{\min} = k_f$, $k_{\max} = k_s$.

4.2 Adjoint problem

The Lagrange multiplier method (Everett 1963) is used to get an optimization problem without constraints and can be used to get the sensitivity of the cost function $\mathcal{J}$. The Lagrangian is defined as

$$\begin{aligned}&\mathcal{L}(\mathbf{u}, p, \theta, \mathbf{u}^*, p^*, \theta^*, \gamma) = \mathcal{J}(\mathbf{u}, p, \theta)\\ &+ \int_\Omega \mathcal{R}(\mathbf{u}, p, \theta)\cdot(\mathbf{u}^*, p^*, \theta^*)\mathrm{d}\Omega,\end{aligned} \tag{14}$$

where $(\mathbf{u}^*, p^*, \theta^*)$ are the so-called adjoint variables and $\mathcal{R}(\mathbf{u}, p, \theta) = 0$ corresponds to the governing (1). In order to compute the adjoint problem for general cost functions, we write the cost functional as follow

$$\mathcal{J}(\mathbf{u}, p, \theta) = \int_\Omega \mathcal{J}_\Omega(\mathbf{u}, p, \theta)\mathrm{d}\Omega + \int_\Gamma \mathcal{J}_\Gamma(\mathbf{u}, p, \theta)\mathrm{d}\Gamma.$$

The critical points of $\mathcal{L}$ with respect to the adjoint variables give the constraint of the optimization problem (4) while the critical point with respect to the primal variable yield the so-called adjoint problem. The latter can be derived as in Othmer (2008) (see also Ramalingom et al. 2018) and is given by

$$\begin{aligned}&\nabla p^* - h_\tau(\gamma)\mathbf{u}^* + \theta\,\nabla\theta^* + \mathrm{A}\,\Delta\mathbf{u}^* + \nabla\mathbf{u}^*\,\mathbf{u}\\ &-(\mathbf{u}^*\cdot\nabla)\mathbf{u} = \frac{\partial\mathcal{J}_\Omega}{\partial\vec{u}}\ \text{in}\ \Omega,\\ &\nabla\cdot\mathbf{u}^* = \frac{\partial\mathcal{J}_\Omega}{\partial p}\ \text{in}\ \Omega,\\ &\mathrm{B}\,\mathbf{u}^*\cdot\overrightarrow{e_y} + \mathbf{u}\cdot\nabla\theta^* + \nabla\cdot(\mathrm{C}\,k_\tau(\gamma)\nabla\theta^*)\\ &= \frac{\partial\mathcal{J}_\Omega}{\partial\theta}\ \text{in}\ \Omega,\end{aligned} \tag{15}$$

together with the boundary conditions for the natural-dominated convection problem

$$\begin{aligned}&\mathbf{u}^* = 0,\ \frac{\partial\mathcal{J}_\Gamma}{\partial\theta} = \mathrm{Re}^{-1}\,\mathrm{Pr}^{-1}\,k_\tau(\alpha)\nabla\theta^*\cdot\mathbf{n},\\ &\partial_n p^* = 0\ \text{on}\ \Gamma_1\cup\Gamma_2,\\ &u_t^* = 0,\ \theta^* = 0,\ \frac{\partial\mathcal{J}_\Gamma}{\partial p} = -u_n^*,\ \partial_n p^* = 0\ \text{on}\ \Gamma_i,\\ &u_t^* = 0\ \text{on}\ \Gamma_o,\\ &\frac{\partial\mathcal{J}_\Gamma}{\partial\theta} = -\theta^*\,u_n - \mathrm{Re}^{-1}\,\mathrm{Pr}^{-1}\,k_\tau(\gamma)\partial_n\theta^*\ \text{on}\ \Gamma_o,\\ &\frac{\partial\mathcal{J}_\Gamma}{\partial\mathbf{u}}\cdot\mathbf{n} = -p^* - \theta^*\,\theta - \mathrm{Re}^{-1}\,\partial_n\mathbf{u}^*\cdot\mathbf{n}\\ &\qquad -u_n^*\,u_n - \mathbf{u}\cdot\mathbf{u}^*\ \text{on}\ \Gamma_o,\end{aligned} \tag{16}$$

where $u_n = \mathbf{u}\cdot\mathbf{n}$ is the normal component of the velocity and $u_t = \mathbf{u}\cdot\vec{t}$ is its tangential part.

In the sequel, we are going to minimize some rescaled cost function (6). We give below the expressions of the derivatives of the cost functions used in the numerical simulations done in the paper, namely the systemic cost functions

$$\hat{\mathcal{J}} = \omega\hat{\mathcal{J}}_1 - (1-\omega)\hat{\mathcal{J}}_2$$

where $\hat{\mathcal{J}}$ is defined with (5) and $\mathcal{J}_1$ and $\mathcal{J}_2$ are given respectively by (8) and (9). Note that, one has

$$\mathcal{J}_\Omega = 0.$$

In addition, the derivatives of $\mathcal{J}_\Gamma$ with respect to the primal variables $(\mathbf{u},\ p,\ \theta)$ are

$$\begin{aligned}\left.\frac{\partial\mathcal{J}\_\Gamma}{\partial p}\right|_{\Gamma_i} &= -\mathrm{c}_1\,\frac{1}{|\Gamma_i|}\int_{\Gamma_i}\mathbf{u}\cdot\mathbf{n}\,\mathrm{d}S\\ \left.\frac{\partial\mathcal{J}_\Gamma}{\partial\theta}\right|_{\Gamma_o} &= \mathrm{c}_2\,\frac{1}{|\Gamma_o|}\int_{\Gamma_o}\mathbf{u}\cdot\mathbf{n}\,\mathrm{d}S\\ \left.\frac{\partial\mathcal{J}_\Gamma}{\partial\mathbf{u}}\right|_{\Gamma_o} &= -\mathrm{c}_1\,\frac{1}{|\Gamma_o|}\mathbf{n}\int_{\Gamma_o}p_t\,\mathrm{d}S - \mathrm{c}_1\,\mathbf{u}\cdot\int_{\Gamma_o}\mathbf{u}\cdot\mathbf{n}\,\mathrm{d}S\\ &\quad + \mathrm{c}_2\,\frac{1}{|\Gamma_o|}\mathbf{n}\int_{\Gamma_o}\theta\,\mathrm{d}S,\end{aligned} \tag{17}$$

where

$$\mathrm{c}_1 = \frac{\omega}{\mathcal{J}_{1,\max} - \mathcal{J}_{1,\min}},\ \mathrm{c}_2 = \frac{-(1-\omega)}{\mathcal{J}_{2,\max} - \mathcal{J}_{2,\min}}.$$

For the systemic cost functions considered in this paper, the adjoint problem is thus given by (15–17) with $\mathcal{J}_\Omega = 0$.

4.3 Implementation

Topology optimization problem is solved by iterative calculations as carried out, for instance, by Ramalingom et al. (2018). The main steps of the algorithm consist to compute sensitivities by adjoint method and evaluate the optimality condition. If a stopping criterion is met, the computations are terminated. For our simulations,

we used the algorithm depicted in (Ramalingom et al. 2018, Page 5, Figure 2) where the stopping criterion is used with $\epsilon = 10^{-7}$. The forward problem (1) and the adjoint problem (15) are implemented using OpenFOAM (Weller et al. 1998). A pressure-based, segregated, steady solver (buoyant-Boussinesq, SimpleFoam) was used with SIMPLE algorithm for pressure-velocity coupling. For all results performed in this paper, we monitored the number of iterations of linear system solver. The generalized Geometric-Algebraic Multi-Grid (GAMG) solver with a cell-centered colocalized finite volume approach is used. Then, the design variables are evaluated by using the conjugated-gradient descent direction method associated to Polack-Ribiere method

$$\beta_{k+1}^{PR} = \frac{\nabla \mathcal{J}_{k+1}^T \left(\nabla \mathcal{J}_{k+1} - \nabla \mathcal{J}_k\right)}{\nabla \mathcal{J}_k^T \, \nabla \mathcal{J}_k}.$$

The gradient of the cost function with respect to the design parameter is given by the critical point of the Lagrangian with respect to the design parameter γ and reads as follows:

$$\begin{aligned} \frac{\partial \mathcal{J}}{\partial \gamma}(\gamma) &= -\frac{\partial h_\tau}{\partial \gamma}\, \mathbf{u}\cdot\mathbf{u}^* - \mathrm{C}\, \frac{\partial k_\tau}{\partial \gamma} \nabla\theta \cdot \nabla\theta^* \quad \text{in } \Omega, \\ \frac{\partial \mathcal{J}}{\partial \gamma}(\gamma) &= -\mathrm{C}\, \frac{\partial k_\tau}{\partial \gamma}\, \theta^* \text{with } \nabla_n \theta = -1 \qquad \text{on } \Gamma_1. \end{aligned} \tag{18}$$

5 Investigated configurations

We present in this section the several cases that are numerically tackled in the paper. We highlight that we are interested in simultaneously minimizing mechanical power and maximizing thermal power in a setting where both of these quantities have the same impact on the optimized vertical channel. As a result, we set

$$\omega = 0.5$$

in all our numerical simulations

Remark 2 We needed to compute the rescaled systemic cost functions $\hat{\mathcal{J}}_1$ and $\hat{\mathcal{J}}_2$ in order to minimize $\hat{\mathcal{J}} = \omega\hat{\mathcal{J}}_1 - (1-\omega)\hat{\mathcal{J}}_2$. As a result, even if these results are not presented here since they are not in the scope of the paper, we actually also solved optimization problem (4) for $\omega = 0$ and $\omega = 1$ hence we minimized the pressure losses and maximized the thermal exchange in the channel.

In Section 6.1, we solve the heat and mass transfer natural convection problem in the asymmetrically heated channel with $\gamma = 0$ in Ω, in order to save references data, for various Ri taken in $\{100, 200, 400\}$ and under constant $\mathrm{Re} = 400$. For these values of Reynolds and Richardson numbers, the conducto-convection problem is dominated by natural convection phenomena. These values have been chosen in accordance with the study of Li et al. (2013) on reversal flows in the asymmetrically heated channel. A vertical velocity profile at the entrance (inlet) of the channel is considered in accordance with the value of $\mathrm{Re} = 400$. Its profile is defined by the following equation:

$$u_i(x) = 6.1x(1-x),$$

where i corresponds to the inlet of the channel. This configuration case is named *Case 1* and the numerical simulation are going to be done without optimization in order to have the values of $\mathcal{J}_1$ and $\mathcal{J}_2$ as reference data and see the influence of adding material in an empty channel on both work of pressure forces and thermal exchange.

In Section 6.2, we compare optimization results obtained with the systemic cost functions (8) and (9) when choosing sigmoid-type functions (11) and (12) with those obtained with Ramp-type functions (13). The comparison is made for Richardson number $\mathrm{Ri} \in \{100, 200, 400\}$. These numerical simulations are referred to as *Case 2*.

In Section 6.3, we solve the optimization problem (4) for $\mathrm{Re} = 400$ and $\mathrm{Ri} = \{100, 200, 400\}$. We used the systemic cost functions given in (8) and (9) and chose sigmoid-type functions (11) and (12) for the interpolations. This study case corresponds to the configuration *Case 3*.

Finally, in Section 6.4, we investigated the topology optimization problem for the case of pure natural convection which is going to be labeled as *Case 4*. We chose various Ra_b numbers taken in $\{3\times10^5, 4\times10^5, 5\times10^5\}$, which corresponds to a laminar flow. We used the systemic cost functions defined in (8) and (9) and chose sigmoid-type functions (11) and (12) for the interpolations.

These four investigated configuration cases are summarized in Table 1.

All optimization results performed in this paper correspond to the thermal and mechanical powers defined as $\mathcal{J}_1$ and $\mathcal{J}_2$. Moreover, in order to be sure that no material is added at the entrance of the channel during the optimization process, we solved the problem by imposing fluid domain at the lower part of the channel, i.e.,

$$\gamma = 0 \text{ for the elements in } [0,1]\times[0,1].$$

We want to enhance heat transfer in the channel and since adding material on the hot plate can affect the heat transfer according to its conductivity, we impose fluid domain near the heated plate. This reads

$$\gamma = 0 \text{ for the elements in } [0, 0.10]\times[2.5, 7.5].$$

It is important to note that the problem is purely academic. In our numerical simulations, the Prandtl number is set to

$$\mathrm{Pr} = 0.71,$$

Table 1 Investigated configuration cases

Case	Case 1	Case 2	Case 3	Case 4
Cost functions	No optimization	$\mathcal{J}_1, \mathcal{J}_2$ (8), (9)	$\mathcal{J}_1, \mathcal{J}_2$ (8), (9)	$\mathcal{J}_1, \mathcal{J}_2$ (8), (9)
Interpolation functions	No optimization	Sigmoid-type and Ramp-type (11), (12),(13)	Sigmoid-type (11), (12)	Sigmoid-type (11), (12)
Natural convection	Re = 400 Ri = {100, 200, 400}	Re = 400 Ri = {100, 200, 400}	Re = 400 Ri = {100, 200, 400}	Ra_b $\{5\ 10^3, 5\ 10^4, 5\ 10^5\}$

which corresponds to a fluid/liquid and the ratio of diffusivity have been therefore set to

$$\frac{k_s}{k_f} = 3.$$

As they are in the range of realistic problems, they are thought to be representative of the problems that can be physically encountered. The parameters appearing in the sigmoïd interpolation function (11) are chosen according to the previous study (Ramalingom et al. 2018). We then take

$$\gamma_0 = 20,\ \tau = 0.6 \text{ and } \gamma_{\max} = 2 \times 10^5,$$

keeping in mind that similar results have been obtained for $\gamma_{\max} = 10^6$.

5.1 Monitored quantities

Thermal quantities are monitored in the heated region and at a discrete vertical coordinate located at the end of the heated plate, namely for $y = 3H/2$ (cf. Fig. 1). The bulk temperature (θ_b), the Nusselt number (Nu_2) at the end of the hot plate $y = 3H/2$, and the local Nusselt number ($\overline{Nu}_1$) integrated along the hot plate are defined as in Desrayaud et al. (2013), respectively:

$$\begin{aligned} \theta_b(y) &= \frac{1}{q_{in}} \int_0^1 u(x,y)\,\theta(x,y)\,\mathrm{d}x,\ \ y = 3H/2 \\ Nu_2(y) &= \frac{1}{\theta(0,y) - \theta_b(y)},\ \ y = 3H/2 \\ \overline{Nu}_1(y) &= \int_{\Gamma_1} \frac{1}{\theta(0,y)}\,dy,\ \ y \in \Gamma_1 \end{aligned} \tag{19}$$

where q_{in} is the mass flow rate entering the channel at $y = 0$.

For each value of Ri and Ra_b, we compute the proportion Q_t of material added in the domain Ω as in Ramalingom et al. (2018):

$$Q_t = \frac{1}{\gamma_{\max}\ V_{tot}} \int_\Omega h_\tau(\gamma)\,\mathrm{d}\Omega, \tag{20}$$

where $V_{tot} = 2\mathrm{Hb}$ is the total volume of Ω.

6 Results and discussion

6.1 Preliminary findings

This section aims to give numerical findings about natural convection in the vertical channel asymmetrically heated (*Case 1*). We consider the single channel with its geometric limitations to solve the problem of natural convection flow in the channel and we model the thermal and dynamic boundary conditions at the exact apertures. The thermal radiations and the heat conduction inside the solid walls are disregarded. According to the results presented by recent studies (Desrayaud et al. 2013; Brangeon et al. 2015; Ramalingom et al. 2017), pressure boundary conditions at the top and bottom sections based on Local Bernoulli relation are chosen in the current numerical study. We compute thermal quantities defined in the previous Section 5.1 without optimization process. These results (cf. Table 2) are going to be used as references within this paper (mentioned as *Case 1*). We solved the problem by using these settings: Re = 400 and Ri = {100, 200, 400}.

We can first observe that $\mathcal{J}_1$ is smaller for Ri = 400, contrarily to $\mathcal{J}_2$ which is bigger. Indeed, Table 2 indicates that the heat transfer in the channel is weaker for Ri = 400 for *Case 1*. So, when natural convection forces are more dominant in our conducto-convection problem, mechanical power increases and thermal power decreases.

Figure 3 shows in blue color negative values of adimensional vertical component of velocity for various Ri. The latter corresponds to the reversal flow which is bigger and larger at the end of the channel when Ri increases. The streamlines (Fig. 3) represent the fluid flow in the channel at various Ri values. So, as highlighted by Desrayaud et al. (2013), the natural convection problem in the vertical channel asymmetrically heated corresponds to a boundary layer flow with a reversal flow at the exit.

6.2 Comparisons between interpolation functions

In this section, we compared the solutions of the optimization problem obtained with the sigmoid functions (11) and

Table 2 Monitored quantities for configuration cases corresponding to constant Re = 400, $\omega = 0.5$, and Ri = {100, 200, 400}, for *Case 1* (without optimization), *Case 2* (sigmoid-type and Ramp-type interpolation functions), and *Case 3* (sigmoid-type interpolation functions)

	θ_b	$Nu_2(3H/2)$	$\overline{Nu}_1$	$\mathcal{J}_1$	$\mathcal{J}_2$	Q_t
Case 1	Without optimization					
Ri = 100	0.01747	12.932	13.611	−5.011	0.0232	Without γ
Ri = 200	0.07015	10.508	7.692	−16.477	0.0888	Without γ
Ri = 400	0.07006	10.510	7.694	−156.12	0.0714	Without γ
Case 2	Comparison between Ramp-type and sigmoid-type interpolation functions					
Ri = 100 sigmoid	0.01759	10.549	12.872	−5.011	0.0232	1.0%
Ri = 200 sigmoid	0.01759	14.349	15.399	−9.173	0.0220	4.1%
Ri = 400 sigmoid	0.01759	16.998	18.904	−17.127	0.0209	8.6%
Ri = 100 Ramp	0.01747	12.932	13.617	−5.010	0.0232	0.2%
Ri = 200 Ramp	0.01746	15.228	14.617	−9.173	0.0220	0.6%
Ri = 400 Ramp	0.01738	17.989	17.641	−17.127	0.0209	0.8%
Case 3	With sigmoid interpolation functions					
Ri = 100	0.01759	12.966	12.873	−5.011	0.0232	1.0%
Ri = 200	0.01744	15.213	15.489	−9.174	0.0219	4.3%
Ri = 400	0.01738	17.992	17.657	−15.427	0.0240	9.6%

(12) and the Ramp functions (13). Parameters for the optimization problems mentioned as *Case 2* are set as follow:

$$\text{Re} = 400,\ \text{Ri} = \{100,\ 200,\ 400\},\ \omega = 0.5.$$

Simulations of these configuration cases with Ramp-type interpolation functions required to add a volume constraint in optimization problem (4)

$$Q_t \leq Q_0,\ Q_0 \in [0, 1],$$

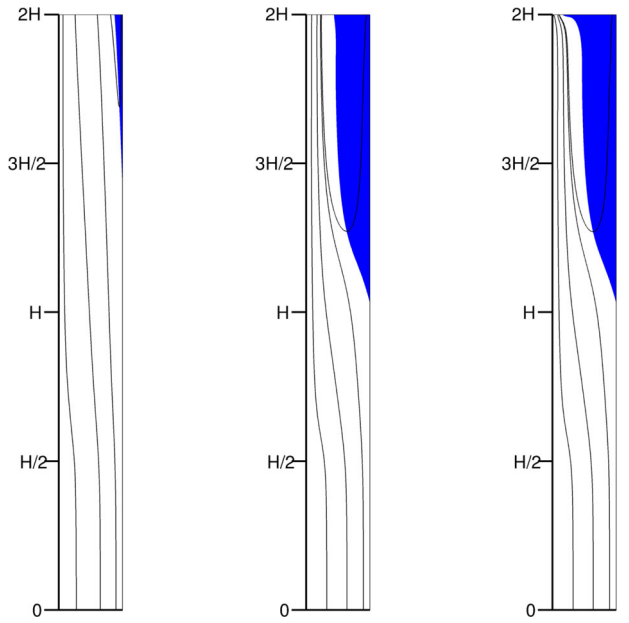

(a) Ri = 100 (b) Ri = 200 (c) Ri = 400

Fig. 3 *Case 1*: Streamlines and reversal flow in blue for Ri = 100 (**a**), Ri = 200 (**b**), and Ri = 400 (**c**)

where Q_t is defined in (20). In our numerical simulations, we chose

$$Q_0 = 0.1,$$

which amounts to fill the channel with at most 10% of solid. To compare the two interpolation functions, we did some numerical experiment (not presented here) using RAMP but without setting a maximal ratio of material in the channel. In such cases, the algorithm filled successively the channel with material before draining it. Therefore, the problem did not give an optimized solution. This is the first noticeable difference between the two types of interpolation function.

In order to correctly make comparisons, we also add the constraint volume for the simulations with sigmoid functions (*Case 2*), i.e., the maximal ratio of material is set to $Q_0 = 0.1$. This parameter corresponds to the maximal global of porosity in Marck et al. (2013), for example.

Secondly, with the Ramp functions, we chose to solve three times the optimization problem since we adopted the strategy from (Borrvall and Petersson 2003; Marck et al. 2013) in order to make the Ramp functions more convex. By varying q parameter in interpolation functions (13), we can tolerate the existence of intermediate states mainly at the beginning of the iterates of the algorithm solving the optimization problem and less at the end. So, parameter q takes successively the values $\{0.01,\ 0.1,\ 1\}$. Likewise, we are going to investigate a continuation strategy for the sigmoid interpolation function and τ is going to take successively the values $\tau \in \{0.6 \times 10^{-4}, 0.6 \times 10^{-3}, 0.6\}$. Figure 4 shows the interpolation functions for these values. As explained by Ramalingom et al. (2018), thanks to the

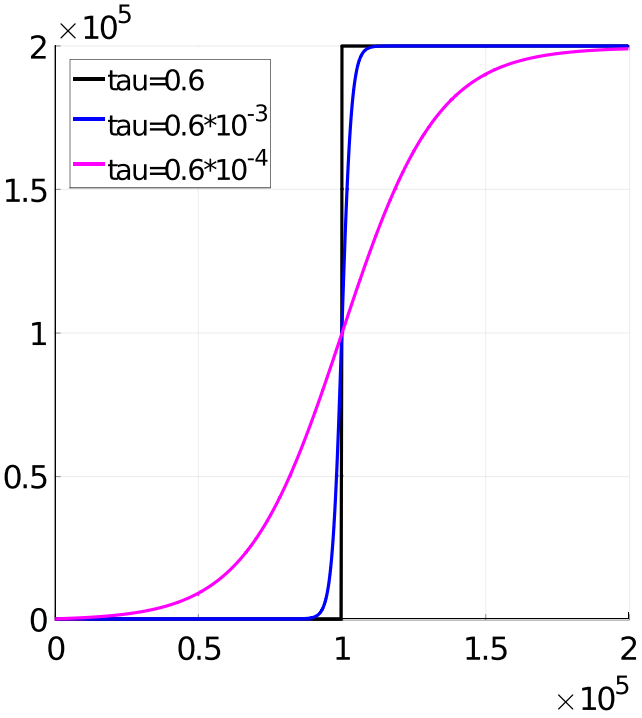

Fig. 4 Interpolation functions for $\tau = \{6 \times 10^{-5}, 6 \times 10^{-4}, 0.6\}$

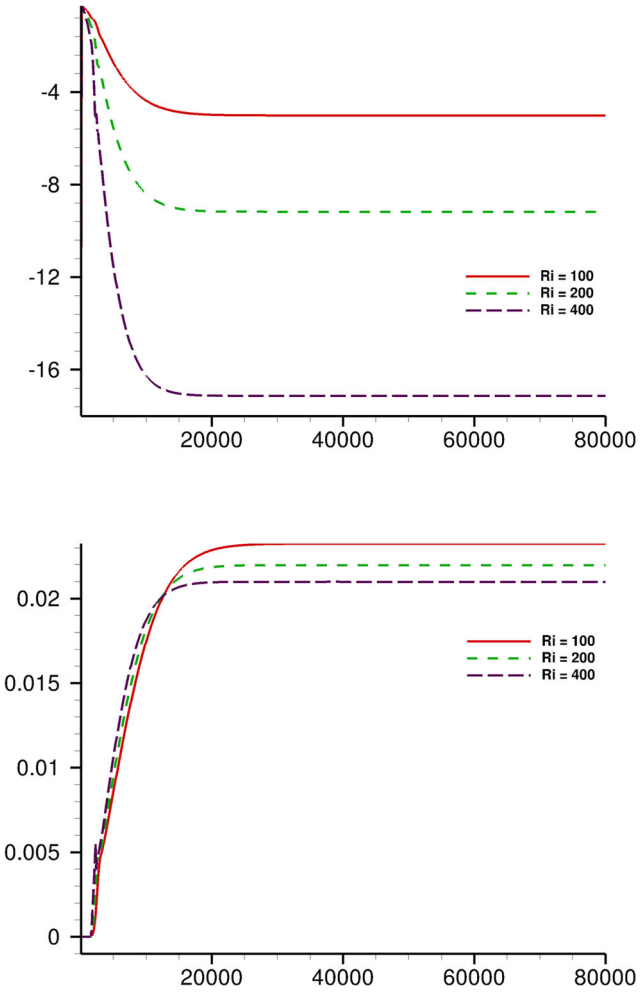

Fig. 5 Evolution of $\mathcal{J}_1$ (top) and $\mathcal{J}_2$ (bottom) over iteration numbers with Ramp-type interpolation functions—*Case 2*

parameter γ_0, we can vary the proportion of material added in the domain by the algorithm.

We represent in Figs. 5 and 6 the evolution of both systemic cost functions over iterations. One can see that, for both interpolation functions, the stopping criterion is reached with a number of iteration that is roughly the same, namely below 20,000. Note that, for Ri $= 100$, the values of $\mathcal{J}_1$ and $\mathcal{J}_2$ after optimization are nearly the same while the other monitored quantities vary. We therefore represent the value of $\hat{\mathcal{J}}$ (see (6)) in Fig. 7 to show that this cost function is indeed minimized and that the number of iteration needed to reach the stopping criterion is again similar for both interpolation functions.

Whichever the interpolation functions chosen, Ramp-type or sigmoid-type, it can be observed that the reversal flow (cf. Fig. 3) is suppressed by the optimized design (cf. Figs. 8 and 9). Indeed, material added by the algorithm at the end of the channel prevent the fluid from re-entering in the channel. Likewise, thermal and mechanical powers are identical to few decimal places at the end of the optimization process (cf. Table 2).

Nevertheless, the structure of material domain obtained is quite different when we use the Ramp-type interpolation functions. The optimized designs obtained in Fig. 9 top contain some holes in which fluid can circulate. Figure 10 is an enlargement of the solid domain at the top-end of the channel in order to see the distribution of solid elements in the optimized designs. However, fluid velocity is zero in this area as shown in Fig. 9 bottom. So, we observe less pieces of isolated material when we solved the optimization problem with the sigmoid-type interpolation functions. The frontier between fluid and solid obtained with the sigmoid-type interpolation functions is smooth.

Finally, heat transfer in the channel is approximately in the same order when the topology optimization problem is solved with the sigmoid-type interpolation functions for any considered Ri. As can be seen in Table 2, for any considered Ri, Nusselt number $\overline{Nu}_1$ computed with sigmoid-type interpolation function records a difference between 5.07 and 6.6% lower compared with $\overline{Nu}_1$ computed with Ramp-type interpolation function.

So, optimization process with sigmoid-type interpolation functions gave smooth shapes as designs obtained did not contain holes in which fluid can circulate. This contribution accounts for an increase of the heat transfer up to 146% compared with the reference *Case 1*.

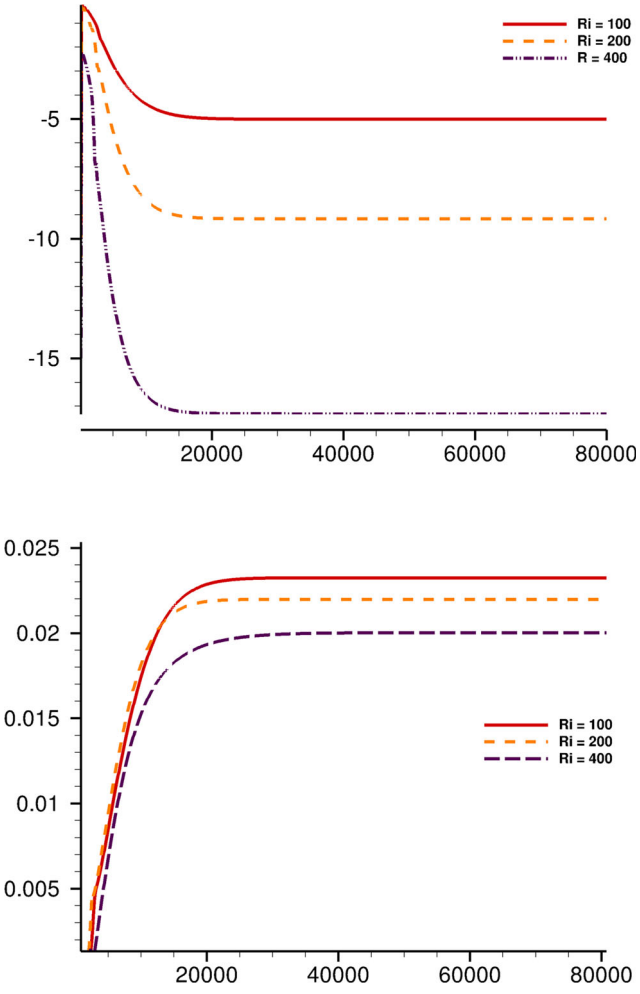

Fig. 6 Evolution of $\mathcal{J}_1$ (top) and $\mathcal{J}_2$ (bottom) over iteration numbers with sigmoid-type interpolation functions, for various Ri, at constant Re = 400. We used a continuation strategy with $\tau \in \{0.6\ 10^{-4}, 0.6\ 10^{-5}, 0.6\}$—*Case 2*

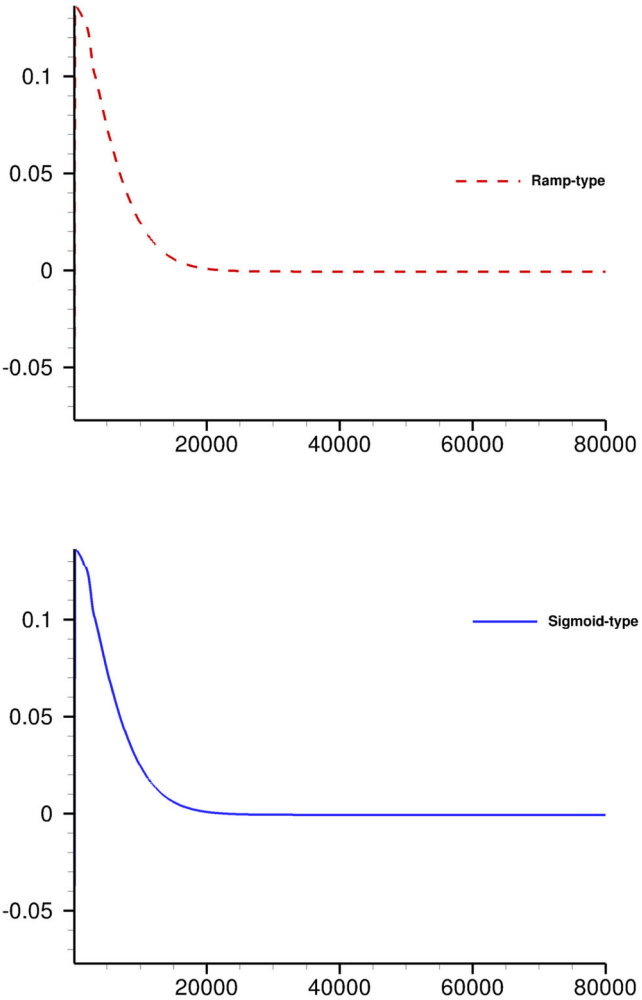

Fig. 7 Evolution of $\hat{\mathcal{J}}$ over iteration numbers for Ri = 100 with Ramp-type (top) and sigmoid-type interpolation functions—*Case 2*

We end this section with some general remarks and comments regarding the results obtained with RAMP and sigmoid interpolation functions. First, as seen from Table 2, the monitored quantities, namely the bulk temperature, the Nusselt numbers, and the values of the cost function at the end of the optimization procedure are slightly the same. As a result, whichever the interpolation technique used, both succeed in reducing pressure losses and maximizing heat transfer in the vertical channel. The major difference is the optimized shape and the quantity of material of the optimized design. Indeed, fluid-solid boundaries of the sigmoid designs are smooth while those obtained with RAMP are defined by multiple holes. Nevertheless, it is worth noting that both designs can be considered very similar in the sense that the zones where the velocity vanishes are nearly the same for both interpolation functions (see Figs. 8 and 9). This observation gives an explanation

Table 3 Monitored quantities for configuration cases corresponding to constant Re = 400, $\omega = 0.5$, and Ri = $\{100, 200, 400\}$, *Case 2* (sigmoid-type and Ramp-type interpolation functions). We used a continuation strategy with $\tau \in \{0.2, 0.4, 0.6\}$

	θ_b	$Nu_2(3H/2)$	$\overline{Nu}_1$	$\mathcal{J}_1$	$\mathcal{J}_2$	Q_t
Case 2						
Ri = 100 sigmoid	0.01750	12.463	14.176	−5.011	0.0232	1.0%
Ri = 200 sigmoid	0.01758	15.247	14.622	−9.174	0.0220	4.3%
Ri = 400 sigmoid	0.01738	17.209	18.533	−15.427	0.0240	9.6%

why they achieved similar performances regarding the monitored quantities from Table 2.

Note also that, thanks to its very sharp nature, the sigmoid interpolation function affect more zones of the computational domain to solid than RAMP. Therefore, RAMP allows less material to be added in order to minimize the cost function than sigmoid. As a result, the sigmoid interpolation function could be considered either as shape optimization or level-set method. However, one major difference is that we do not need any mesh refinement

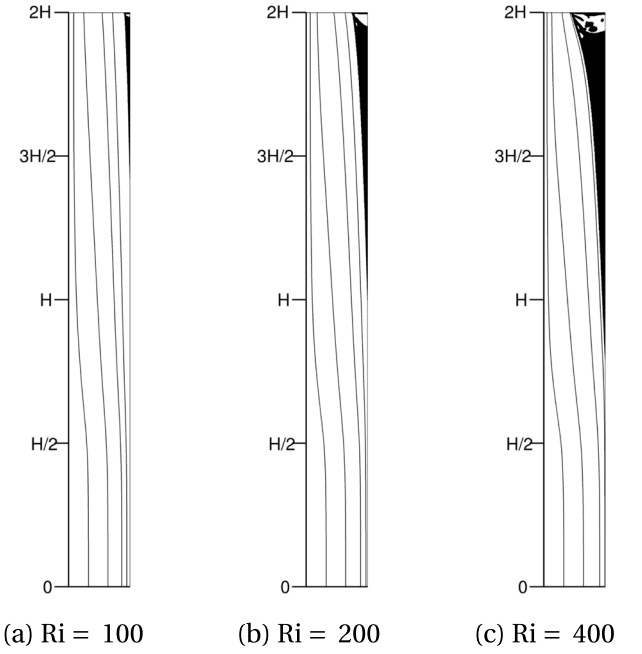

(a) Ri = 100 (b) Ri = 200 (c) Ri = 400

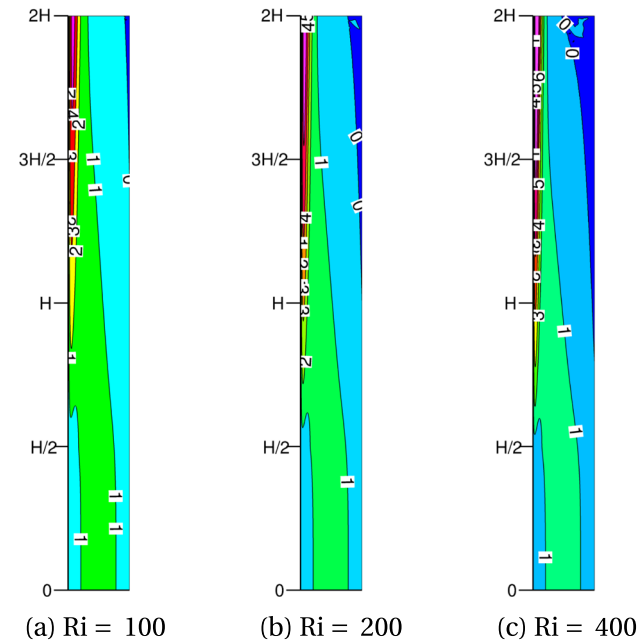

(a) Ri = 100 (b) Ri = 200 (c) Ri = 400

Fig. 8 $h_\tau(\gamma)$ and streamtraces (top), adimensional vertical velocity component (bottom) obtained with sigmoid-type interpolation functions for various Ri and continuation approach for $\tau \in \{0.6 \times 10^{-5}, 0.6 \times 10^{-4}, 0.6\}$—*Case 2* with sigmoid interpolation functions. **a** Ri = 100. **b** Ri = 200. **c** Ri = 400

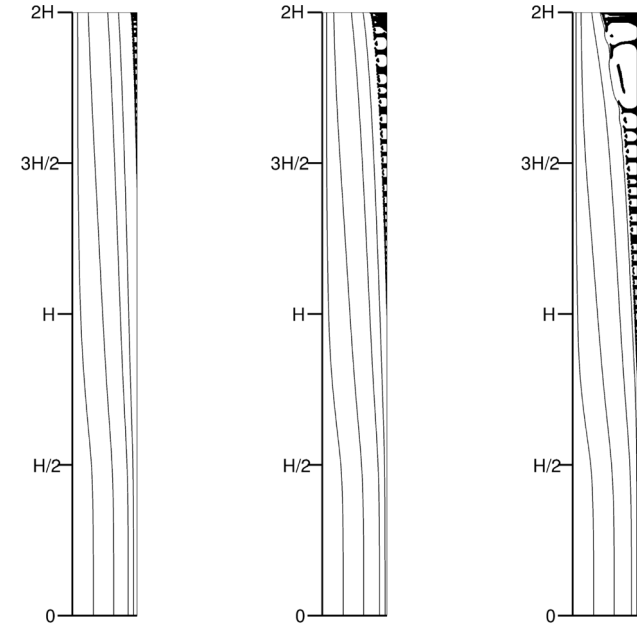

(a) Ri = 100 (b) Ri = 200 (c) Ri = 400

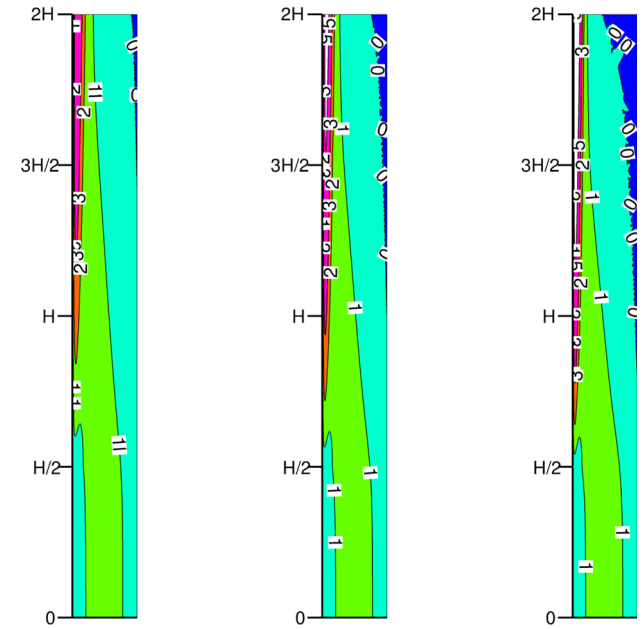

(a) Ri = 100 (b) Ri = 200 (c) Ri = 400

Fig. 9 $h_\tau(\gamma)$ and streamtraces (top), adimensional vertical velocity component (bottom) obtained with Ramp-type interpolation functions, for various Ri—*Case 2* with Ramp interpolation functions. **a** Ri = 100. **b** Ri = 200. **c** Ri = 400

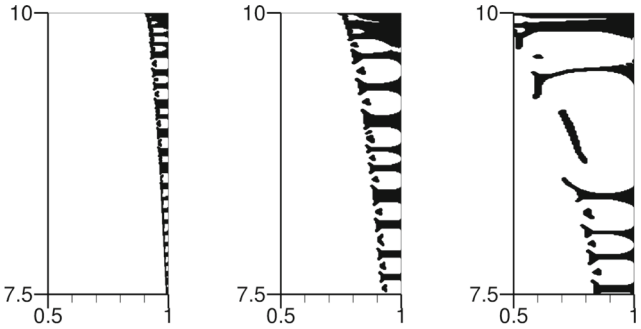

(a) Ri = 100 (b) Ri = 200 (c) Ri = 400

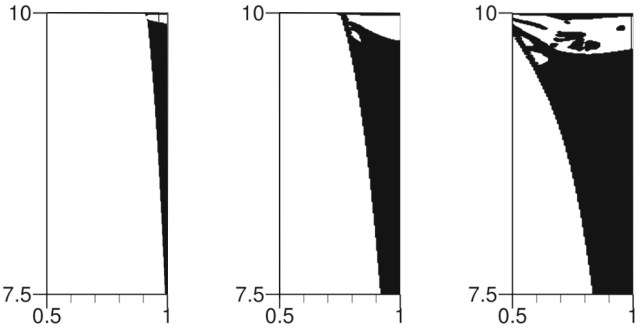

(a) Ri = 100 (b) Ri = 200 (c) Ri = 400

Fig. 10 Zoom on the solid domain obtained with Ramp-type (top) and with sigmoid-type (bottom) interpolation functions for various Ri—*Case 2*. **a** Ri = 100. **b** Ri = 200. **c** Ri = 400

techniques. In addition, we have the parameter τ at hand that can still be tuned to have non-sharp interpolation function which, even if they cannot be convex as RAMP, could still achieved more complex designs. The latter is however beyond the scope of the paper which was formerly intended to solve topology optimization problem for buoyancy-driven flows by introducing new cost functions.

Remark 3 (**Comparison between two continuation strategies**) We also did numerical simulations with a continuation strategy with $\tau \in \{0.2, 0.4, 0.6\}$. This amounts to start with a very sharp interpolation function. With these values, we obtain roughly the same monitored quantity as those we get without continuation strategy and $\tau = 0.6$ which is so-called *Case 3* (compare *Case 3* from Table 2 with Table 3). We emphasize that the quantity of material is roughly the same as well as the designs (see Fig. 11 for *Case 3*) and we thus do not show them.

It is worth noting that the monitored quantities are slightly the same whatever the parameters used in the continuation strategy (compare *Case 2* from Table 2 with Table 3). The only real difference is that some piece of isolated material disappear, namely some zones where the velocity of the fluid vanishes are filled with solid, when using the continuation strategy with $\tau \in \{0.2, 0.4, 0.6\}$ (compare Figs. 10 and 11). This fact and since the sigmoid with $\tau \geq 0.2$ is sharper than with $\tau \geq 6 \times 10^{-5}$ actually explain why the quantity of material increases in

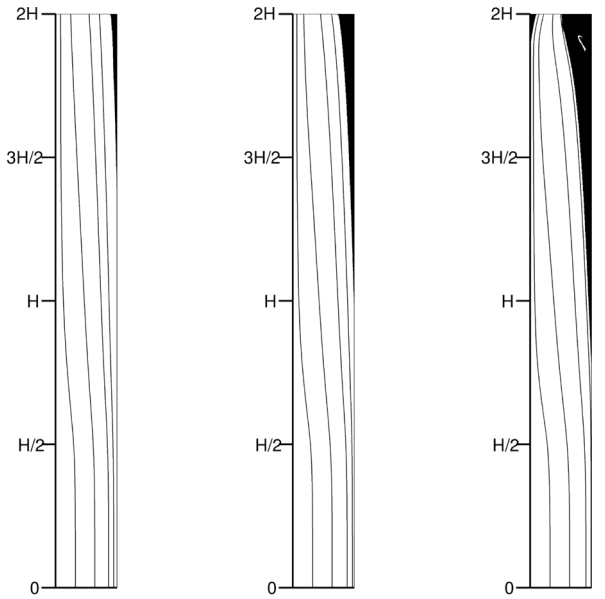

(a) Ri = 100 (b) Ri = 200 (c) Ri = 400

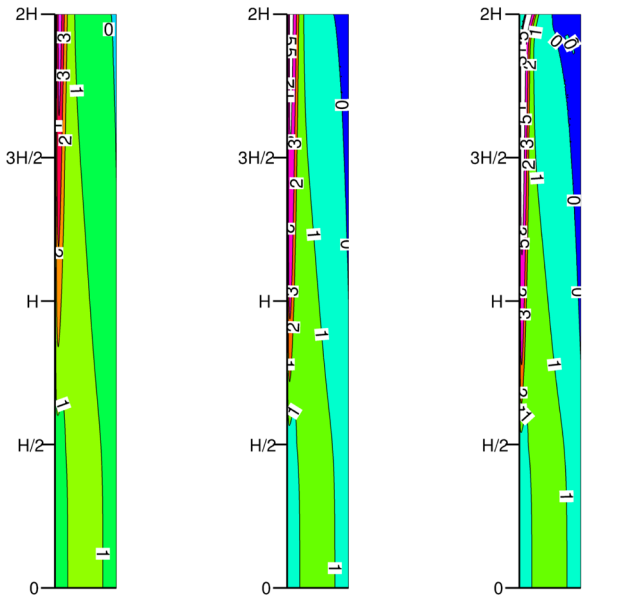

(a) Ri = 100 (b) Ri = 200 (c) Ri = 400

Fig. 11 $h_\tau(\gamma)$ and streamtraces (top), adimensional vertical velocity component (bottom) obtained for various Ri—*Case 3*. **a** Ri = 100. **b** Ri = 200. **c** Ri = 400

Table 4 Monitored quantities for pure natural convection configuration case at various Ra_b—*Case 4*

	θ_b	$Nu_2(3H/2)$	$\overline{Nu}_1$	$\mathcal{J}_1$	$\mathcal{J}_2$	Q_t
	Case 5: pure natural convection case without optimization					
$Ra_b = 5 \times 10^3$	0.18709	4.275	3.330	−0.028	0.0707	Without γ
$Ra_b = 5 \times 10^4$	0.09002	5.633	4.939	−0.008	0.0222	Without γ
$Ra_b = 5 \times 10^5$	0.06617	5.140	7.273	−5.5e−04	0.0071	Without γ
	Case 4: pure natural convection case					
$Ra_b = 5 \times 10^3$	0.18712	4.333	3.311	−0.076	0.0707	0%
$Ra_b = 5 \times 10^4$	0.08884	5.625	4.969	−0.038	0.0222	2.21%
$Ra_b = 5 \times 10^5$	0.05072	5.986	7.451	−0.013	0.0070	5.37%

this case and why the monitored quantities does not vary significantly.

Regarding the continuation strategy, since differences between the monitored quantity for the two set of τ used does not have significant differences with respect to those computed with only $\tau = 0.6$ (see Remark 3), we chose to not use such continuation strategy in the two next sections. To conclude this section, both interpolation techniques have pros and cons and, since the results are either slightly the same or can be linked together, we choose to work with the sigmoid in the remaining sections of this paper.

6.3 Topology optimization problem for constant Re = 400 and various Ri

This section presents the solution of the optimization problem for various Ri. We used the systemic cost functions given in (8) and (9) and chose sigmoid-type functions (11) and (12) for the interpolations. This study case corresponds to the configuration *Case 3*.

Figure 12 represents the evolution of $\mathcal{J}_1$ and $\mathcal{J}_2$ over iterations for various Ri. One can then see that our algorithm succeeds to minimize/maximize one or other cost functions for any Ri. We observe that mechanical power decreases over iterations while thermal power increases. So, our algorithm succeeds to converge to an optimized solution for this studied case.

It can be observed that optimized design suppresses the reversal flow (cf. Fig. 3) as seen in previous studied case. Moreover, the domain material at the end of the optimization corresponds to the reversal flow represented in Fig. 3. Finally, as one can see from Fig. 11, adimensional vertical component of the velocity has a positive value in the channel after optimization and vanishes or is about 5.5×10^{-5} which is small enough for this zone to be considered as solid. Our objective functions give an optimized design with no physical error as a non-null velocity in the solid regions without connectivity as mentioned by Kreissl and Maute (2012) and Lee (2012).

Concerning the quantity of material added in the channel, the optimization algorithm tends to add more material in the domain (cf. Fig. 11 top) when Ri increases. This proportion of material is about 9.6% of the domain when Ri = 400 and contributes to modifying the circulation of the flow in the channel, as the fluid is closer to the heated wall. So, in

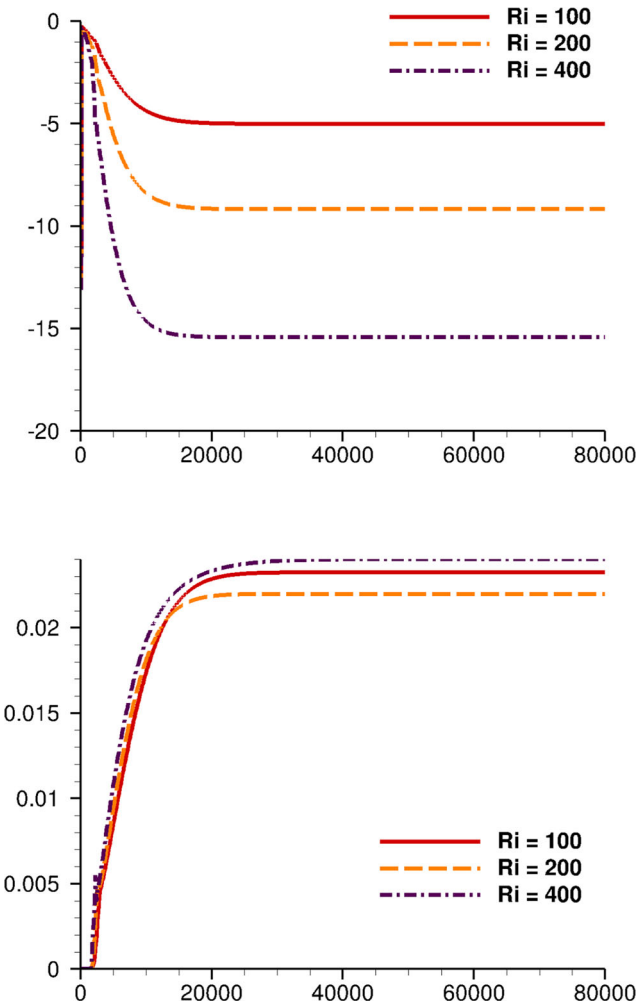

Fig. 12 Evolution of $\mathcal{J}_1$ (top) and $\mathcal{J}_2$ (bottom) over iteration numbers with sigmoid-type interpolation functions—*Case 3*

order to minimize mechanical power and maximize thermal power, the strategy of algorithm consists in suppressing the reversal flow at the end of the channel and adding material so as to oblige the fluid flow near the heated wall. Besides, Table 2 shows that the mean Nusselt number $\overline{Nu}_1$ is multiplied by a factor 2.3 after optimization for Ri $= 400$. Likewise, the Nusselt number at the end of the hot plate $Nu_2(3H/2)$ is multiplied by a factor 1.7 after optimization for Ri $= 400$. Therefore, Nusselt numbers increased when Ri increased, so the heat transfer is correctly enhanced in the optimized design obtained. Nevertheless, this addition of material contributes to reducing strongly $\mathcal{J}_1$ for small improvements of $\mathcal{J}_2$ (cf. Fig. 12). This situation has already been observed by Pietropaoli et al. (2019) who noticed in their study in forced convection some small improvements on the heat exchange efficiency while pressure drop remains relatively high.

6.4 Topology optimization problem in case of pure natural convection for various Ra_b

This section presents the solutions of the optimization problem in case of pure natural convection. We used the sigmoid-type interpolation functions and solve the optimization problem (3) without adding the constraint of volume. So the proportion of material is just controlled with parameters $\gamma_0 = 20$ of the sigmoid interpolation functions. We set the Rayleigh number Ra_b to different values:

$$\mathrm{Ra}_b \in \{3 \times 10^5,\ 4 \times 10^5,\ 5 \times 10^5\}.$$

As previously mentioned, the pure natural convection topology optimization problem is furthermore solved without optimization process. The references monitored quantities are showed in Table 4.

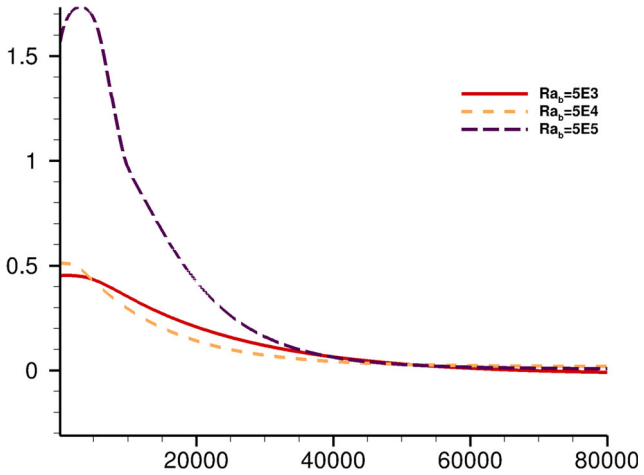

Fig. 13 Evolution of $\hat{\mathcal{J}}$ over iteration numbers with sigmoid-type interpolation functions, for various Ra_b numbers—*Case 4*

Figure 13 represents the evolution of $\hat{\mathcal{J}}$ over iterations for various Ra_b. One can see the convergence of the algorithm for any Ra_b.

Figure 14 shows the optimized designs obtained at various Ra_b. The optimization algorithm adds few quantity of material in the domain, less than 6% (cf. Table 4). When no reversal flow exists, in particular for $\mathrm{Ra}_b = 3 \times 10^5$, the optimization algorithm did not add material in the domain. Also, as seen with the previous configuration cases, the fluid flow structure is thus modified and vertical component

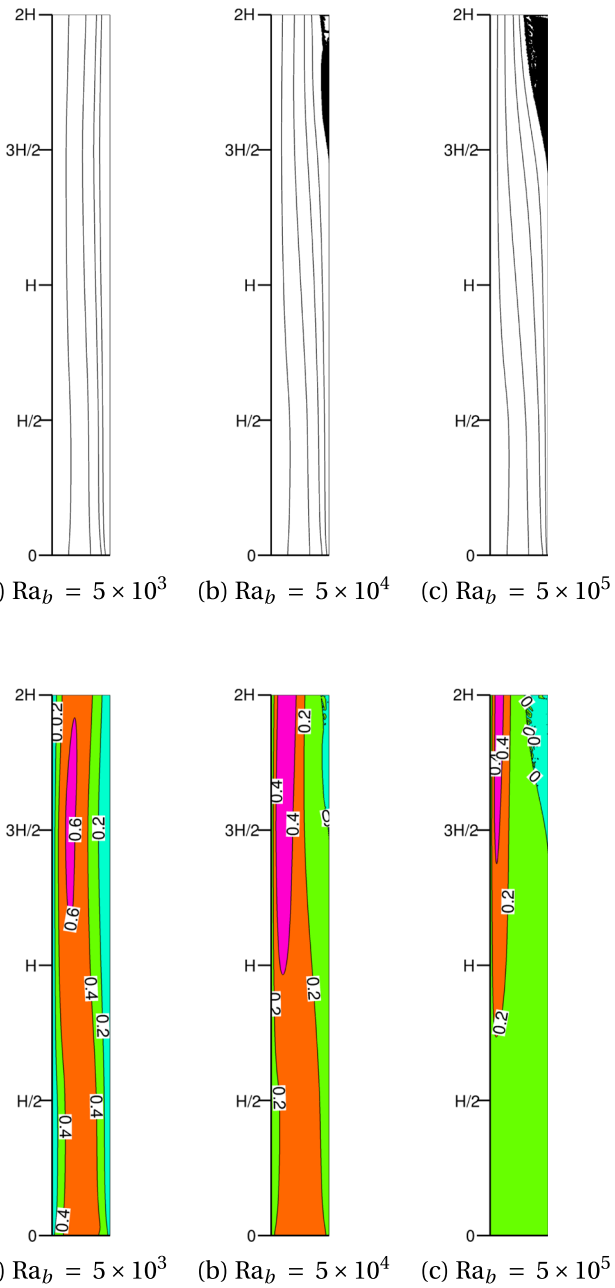

Fig. 14 $h_\tau(\gamma)$ and streamtraces obtained for various Ra_b (top), adimensional vertical velocity component obtained for various Ra_b (bottom)—*Case 4*. **a** $\mathrm{Ra}_b = 5 \times 10^3$. **b** $\mathrm{Ra}_b = 5 \times 10^4$. **c** $\mathrm{Ra}_b = 5 \times 10^5$

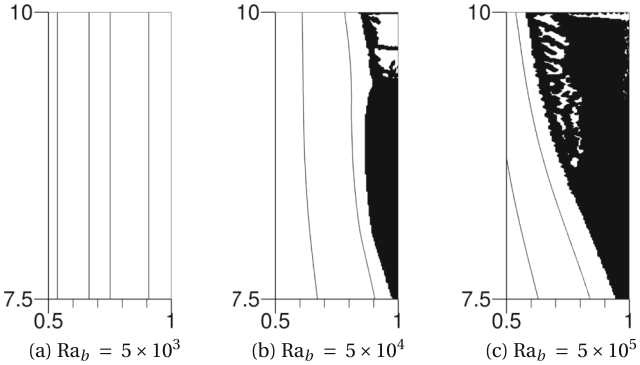

(a) $\mathrm{Ra}_b = 5 \times 10^3$ (b) $\mathrm{Ra}_b = 5 \times 10^4$ (c) $\mathrm{Ra}_b = 5 \times 10^5$

Fig. 15 Zoom on the solid domain obtained for the configuration case of pure natural convection—*Case 4*. **a** $\mathrm{Ra}_b = 5 \times 10^3$. **b** $\mathrm{Ra}_b = 5 \times 10^4$. **c** $\mathrm{Ra}_b = 5 \times 10^5$

of the velocity is not negative yet (cf. Fig. 14 bottom). Moreover, when we enlarge the top-end of the optimized designs in Fig. 15, we can observe the presence of fluid holes without solid matrix in the material domain acting as isolation from the fluid. This composite material constitutes an insulation as its global conductivity tends to the one of the fluid. The heat transfer in the channel is quite weak compared with previous studied cases (*Case 3*), less than 2.5% for values of Ra_b compared with the reference study case.

Therefore, when Ra_b increases, which corresponds to an increase of thermal flux at the hot plate of the channel, the algorithm adds more material at the top-end of the channel in order to suppress the reversal flow (which contributes to reduce $\mathcal{J}_1$) and to force the fluid circulation closed the hot plate. Indeed, Fig. 15 indicates material takes up about the half width of the channel, above the hot plate. This strategy increases the fluid velocity in this Section 14 bottom, and so the Nusselt number $Nu_2(3H/2)$.

7 Conclusion

An optimization problem considering both pressure drop minimization and heat transfer maximization in the asymmetrically heated channel has been examined. After discussing some limits, we identified for classical pressure-drop cost functions, two objective functions are investigated representing the work of pressure forces for the mechanical power and heat exchanges with the thermal power. These functions allow to obtain optimal designs and they are reduced for all values of Richardson number and Rayleigh numbers considered in this study. Two different types of interpolation function are applied and compared: Ramp-type and sigmoid-type. They have pros and cons and, since the results are either slightly the same or can be linked together, they can be freely chosen for dealing with natural convection topology optimization problem. Then, the problem is handled in natural convection for constant Reynolds number set to 400 and several values of Richardson number taken in $\{100, 200, 400\}$. Second, the problem is handled in pure natural convection with various values of modified Rayleigh number taken in $\{5 \times 10^3, 5 \times 10^4, 5 \times 10^5\}$. Several conclusions have been drawn. First of all, the optimized design suppresses the reversal flow in the channel. That contributes to reduce pressure losses and modify the circulation of fluid in the channel. Then, the new expressions of cost functions converge over with a number of iterations which are similar for both interpolation functions while the optimized designs show a better connectivity of the solid region when using the sigmoid. Values of mechanical power and thermal power are closed for both interpolation function used. Moreover, this approach that consists of dissociating quantities in the expression of cost functions by considering average quantities is well adapted to natural convection phenomena. In case of pure natural convection, when the fluid flow is laminar, the algorithm adds less than 6% of material and we obtain composite material which acts as an insulating. Finally, thermal exchanges are evaluated by the calculation of Nusselt number at the hot plate and based on the bulk temperature. The optimization algorithm is able to increase thermal exchanges while maintaining the pressure losses due to friction, thanks to the combined objective functions used. Nevertheless, the reduction of losses of charge is more significant than the improvement of heat transfer. In conclusion, this study highlights the importance of the expression of cost functions in a topology optimization problem, dominated by natural convection forces. The influence of the Richardson is observed on the quantity of material added in the optimized channel. As future work, we suggest a more complete heat and mass transfer model to be considered, as pure natural convection problems in unsteady regime and radiation problems.

Acknowledgments Computations have been performed on the University of Reunion Island supercomputer facility.

Compliance with Ethical Standards

Conflict of interest The authors declare that they have no conflict of interest.

References

Alexandersen J, Andreasen CS, Aage N, Lazarov BS, Sigmund O (2013) Topology optimisation for coupled convection problems. In: 10th World Congress on Structural and Multidisciplinary Optimization, Orlando, pp 19–24

Alexandersen J, Aage N, Andreasen CS, Sigmund O (2014) Topology optimisation for natural convection problems. Int J Numer Methods Fluids 76(10):699–721

Alexandersen J, Sigmund O, Aage N (2015) Topology optimisation of passive coolers for light-emitting diode lamps. In: 11th World Congress on Structural and Multidisciplinary Optimization

Alexandersen J, Sigmund O, Aage N (2016) Large scale three-dimensional topology optimisation of heat sinks cooled by natural convection. Int J Heat Mass Transfer 100:876–891

Alexandersen J, Sigmund O, Meyer KE, Lazarov BS (2018) Design of passive coolers for light-emitting diode lamps using topology optimisation. Int J Heat Mass Transfer 122:138–149

Asmussen J, Alexandersen J, Sigmund O, Andreasen CS (2018) A "poor man's" approach to topology optimization of natural convection problems. arXiv:180901900

Athan TW, Papalambros PY (1996) A note on weighted criteria methods for compromise solutions in multi-objective optimization

Aung W (1972) Fully developed laminar free convection between vertical plates heated asymmetrically. Int J Heat Mass Transfer 15(8):1577–1580

Aung W, Fletcher L, Sernas V (1972) Developing laminar free convection between vertical flat plates with asymmetric heating. Int J Heat Mass Transfer 15(11):2293–2308

Bar-Cohen A, Rohsenow W (1984) Thermally optimum spacing of vertical, natural convection cooled, parallel plates. Journal of heat transfer 106(1):116–123

Bastide A, Cocquet PH, Ramalingom D (2018) Penalization model for navier-stokes-darcy equation with application to porosity-oriented topology optimization. Mathematical Models and Methods in Applied Sciences, https://doi.org/10.1142/S0218202518500409

Bendsøe MP, Kikuchi N (1988) Generating optimal topologies in structural design using a homogenization method. Comput Methods Appl Mech Eng 71(2):197–224

Bodoia J, Osterle J (1962) The development of free convection between heated vertical plates. J Heat Transf 84(1):40–43

Borrvall T, Petersson J (2003) Topology optimization of fluids in stokes flow. Int J Numer Methods Fluids 41(1):77–107

Brangeon B, Joubert P, Bastide A (2015) Influence of the dynamic boundary conditions on natural convection in an asymmetrically heated channel. Int J Therm Sci 95:64–72

Bruns T (2005) A reevaluation of the simp method with filtering and an alternative formulation for solid–void topology optimization. Struct Multidiscip Optim 30(6):428–436

Bruns TE (2007) Topology optimization of convection-dominated, steady-state heat transfer problems. Int J Heat Mass Transfer 50(15-16):2859–2873

Coffin P, Maute K (2016) Level set topology optimization of cooling and heating devices using a simplified convection model. Struct Multidiscip Optim 53(5):985–1003

Dbouk T (2017) A review about the engineering design of optimal heat transfer systems using topology optimization. Appl Therm Eng 112:841–854

Dede EM (2009) Multiphysics topology optimization of heat transfer and fluid flow systems. In: Proceedings of the COMSOL Users Conference

Desrayaud G, Lauriat G (2009) Flow reversal of laminar mixed convection in the entry region of symmetrically heated, vertical plate channels. Int J Therm Sci 48(11):2036–2045

Desrayaud G, Chénier E, Joulin A, Bastide A, Brangeon B, Caltagirone J, Cherif Y, Eymard R, Garnier C, Giroux-Julien S et al (2013) Benchmark solutions for natural convection flows in vertical channels submitted to different open boundary conditions. Int J Therm Sci 72:18–33

Elenbaas W (1942) Heat dissipation of parallel plates by free convection. Physica 9(1):1–28

Eschenauer HA, Olhoff N (2001) Topology optimization of continuum structures: a review. Appl Mech Rev 54(4):331–390

Everett H III (1963) Generalized Lagrange multiplier method for solving problems of optimum allocation of resources. Oper Res 11(3):399–417

Goeke S, Wünsch O (2017) Adjoint based topology optimization of conjugate heat transfer systems. PAMM 17(1):771–772

Guest JK, Prévost JH, Belytschko T (2004) Achieving minimum length scale in topology optimization using nodal design variables and projection functions. Int J Numer Methods Eng 61(2):238–254

Haertel JH, Nellis GF (2017) A fully developed flow thermofluid model for topology optimization of 3d-printed air-cooled heat exchangers. Appl Therm Eng 119:10–24

Haertel JHK, Engelbrecht K, Lazarov BS, Sigmund O (2015) Topology optimization of thermal heat sinks. In: Proceedings of the 2015 COMSOL Conference, Grenoble

Hassani B, Hinton E (1998a) A review of homogenization and topology opimization ii—analytical and numerical solution of homogenization equations. Compos Struct 69(6):719–738

Hassani B, Hinton E (1998b) A review of homogenization and topology optimization i—homogenization theory for media with periodic structure. Compos Struct 69(6):707–717

Hassani B, Hinton E (1998c) A review of homogenization and topology optimization iii—topology optimization using optimality criteria. Compos Struct 69(6):739–756

Joo Y, Lee I, Kim SJ (2017) Topology optimization of heat sinks in natural convection considering the effect of shape-dependent heat transfer coefficient. Int J Heat Mass Transfer 109:123–133

Koga AA, Lopes ECC, Nova HFV, de Lima CR, Silva ECN (2013) Development of heat sink device by using topology optimization. Int J Heat Mass Transfer 64:759–772

Kontoleontos E, Papoutsis-Kiachagias E, Zymaris A, Papadimitriou D, Giannakoglou K (2013) Adjoint-based constrained topology optimization for viscous flows, including heat transfer. Eng Optim 45(8):941–961

Kreissl S, Maute K (2012) Levelset based fluid topology optimization using the extended finite element method. Struct Multidiscip Optim 46(3):311–326

Lazarov BS, Sigmund O (2011) Filters in topology optimization based on helmholtz-type differential equations. Int J Numer Methods Eng 86(6):765–781

Lee K (2012) Topology optimization of convective cooling system designs. PhD thesis, University of Michigan

Lei T, Alexandersen J, Lazarov BS, Wang F, Haertel JH, De Angelis S, Sanna S, Sigmund O, Engelbrecht K (2018) Investment casting and experimental testing of heat sinks designed by topology optimization. Int J Heat Mass Transfer 127:396–412

Li R, Bousetta M, Chénier E, Lauriat G (2013) Effect of surface radiation on natural convective flows and onset of flow reversal in asymmetrically heated vertical channels. Int J Therm Sci 65:9–27

Liang QQ (2007) Performance-based optimization: a review. Adv Struct Eng 10(6):739–753

Lim DK, Park Y, Kim H et al (2018) CFD-based shape optimization on cross-section of monoblock fusion divertor cooling channel for minimizing local heat flux. Fusion Eng Des 136:1100–1105

Lv Y, Liu S (2018) Topology optimization and heat dissipation performance analysis of a micro-channel heat sink. Meccanica 53(15):3693–3708

Marck G, Nemer M, Harion JL (2013) Topology optimization of heat and mass transfer problems: laminar flow. Numerical Heat Transfer Part B: Fundamentals 63(6):508–539

Messac A, Puemi-Sukam C, Melachrinoudis E (2000) Aggregate objective functions and pareto frontiers: required relationships and practical implications. Optim Eng 1(2):171–188

Morrison AT (1992) Optimization of heat sink fin geometries for heat sinks in natural convection. In: Thermal Phenomena in Electronic Systems, 1992. i-THERM III, InterSociety Conference on. IEEE, pp 145-148

Nasri Z, Laatar AH, Balti J (2015) Natural convection enhancement in an asymmetrically heated channel-chimney system. Int J Therm Sci 90:122–134

Othmer C (2008) A continuous adjoint formulation for the computation of topological and surface sensitivities of ducted flows. Int J Numer Methods Fluids 58(8):861–877

Othmer C (2014) Adjoint methods for car aerodynamics. J Math Ind 4(1):6

Othmer C, Kaminski T, Giering R (2006) Computation of topological sensitivities in fluid dynamics: cost function versatility. In: ECCOMAS CFD 2006: Proceedings of the European Conference on Computational Fluid Dynamics, Egmond aan Zee, The Netherlands, September 5-8, Citeseer, pp 1–12

Papoutsis-Kiachagias EM, Giannakoglou KC (2016) Continuous adjoint methods for turbulent flows, applied to shape and topology optimization: industrial applications. Arch Comput Meth Eng 23(2):255–299

Pietropaoli M, Montomoli F, Gaymann A (2019) Three-dimensional fluid topology optimization for heat transfer. Struct Multidiscip Optim 59(3):801–812

Qian X, Dede EM (2016) Topology optimization of a coupled thermal-fluid system under a tangential thermal gradient constraint. Struct Multidiscip Optim 54(3):531–551

Ramalingom D, Cocquet PH, Bastide A (2017) Numerical study of natural convection in asymmetrically heated channel considering thermal stratification and surface radiation. Numerical Heat Transfer Part A: Applications 72(9):681–696

Ramalingom D, Cocquet PH, Bastide A (2018) A new interpolation technique to deal with fluid-porous media interfaces for topology optimization of heat transfer. Comput Fluids 168:144–158

Rokicki J et al (2016) Adjoint lattice boltzmann for topology optimization on multi-gpu architecture. Computers & Mathematics with Applications 71(3):833–848

Saglietti C, Schlatter P, Monokrousos A, Henningson DS (2017) Adjoint optimization of natural convection problems: differentially heated cavity. Theor Comput Fluid Dyn 31(5-6):537–553

Saglietti C, Wadbro E, Berggren M, Henningson D (2018) Heat transfer maximization in a three dimensional conductive differentially heated cavity by means of topology optimization. In: Proceedings of the Seventh European Conference on Computational Fluid Dynamics (ECCM-ECFD)

Sanvicente E, Giroux-Julien S, Ménézo C, Bouia H (2013) Transitional natural convection flow and heat transfer in an open channel. Int J Therm Sci 63:87–104

Sigmund O (2007) Morphology-based black and white filters for topology optimization. Struct Multidiscip Optim 33(4-5):401–424

Sigmund O, Maute K (2012) Sensitivity filtering from a continuum mechanics perspective. Struct Multidiscip Optim 46(4):471–475

Sigmund O, Maute K (2013) Topology optimization approaches

Talukdar D, Li CG, Tsubokura M (2019) Investigation on optimization of the thermal performance for compressible laminar natural convection flow in open-ended vertical channel. Int J Heat Mass Transfer 128:794–806

Thebault M, Giroux-Julien S, Menezo C, Timchenko V (2017) Natural convective flow analysis in vertical channel. In: ICHMT DIGITAL LIBRARY ONLINE, Begel House Inc

Tkachenko O, Timchenko V, Giroux-Julien S, Ménézo C, Yeoh G, Reizes J, Sanvicente E, Fossa M (2016) Numerical and experimental investigation of unsteady natural convection in a non-uniformly heated vertical open-ended channel. Int J Therm Sci 99:9–25

Tong ZX, Li MJ, Yan JJ, Tao WQ (2018) Optimizing thermal conductivity distribution for heat conduction problems with different optimization objectives. Int J Heat Mass Transfer 119:343–354

Wang MY, Wang X, Guo D (2003) A level set method for structural topology optimization. Comput Methods Appl Mech Eng 192(1-2):227–246

Weller GH, Tabor G, Jasak H et al (1998) A tensorial approach to computational continuum mechanics using object-oriented techniques. Comput Phys 12.6:620–631

Yaji K, Yamada T, Yoshino M, Matsumoto T, Izui K, Nishiwaki S (2016) Topology optimization in thermal-fluid flow using the lattice boltzmann method. J Comput Phys 307:355–377

Yoon GH (2010) Topological design of heat dissipating structure with forced convective heat transfer. J Mech Sci Technol 24(6):1225–1233

Zhao X, Zhou M, Sigmund O, Andreasen CS (2018) A "poor man's approach" to topology optimization of cooling channels based on a darcy flow model. Int J Heat Mass Transfer 116:1108–1123

Zhou M, Rozvany G (1991) The coc algorithm, part ii: topological, geometrical and generalized shape optimization. Comput Methods Appl Mech Eng 89(1-3):309–336